Introduction

Tumor necrosis factor (TNF) mediates resistance to tuberculosis. Excess TNF production, however, is detrimental because it induces pathogenic necrosis of infected macrophages in the tuberculous granuloma, which releases the mycobacteria into the extracellular milieu, promoting their growth and transmission to new hosts. Excess TNF, through the kinase RIP3 and the mitochondrial phosphatase PGAM5, increases reactive oxygen species such as superoxide and hydrogen peroxide in the mitochondria of mycobacterium-infected macrophages. These mitochondrial reactive oxygen species (mROS) initiate an elaborate interorganellar signaling circuit that ultimately causes macrophage necrosis and release of mycobacteria.

Rationale

How TNF signaling elevates mROS production is not known. To address this question in vivo, we used zebrafish larvae, taking advantage of their optical transparency and their amenability to genetic and pharmacological manipulation. Thus, we could visualize and quantify mROS and macrophage necrosis after these manipulations.

Results

Typically, mROS are generated during normal respiration when electrons from NADH, produced by metabolic pathways, enter the electron transport chain (ETC) and are transferred by forward electron transport from complex I to coenzyme Q (CoQ). We found that in wild-type animals (without excess TNF), mycobacterial infection induced a small boost in multiple metabolic pathways that increased mROS through this process. This slight increase in mROS did not result in macrophage necrosis. In animals with excess TNF (TNF^{hi} animals), we found that the greatly increased mROS were not induced through conventional forward electron transport but rather through reverse electron transport (RET). RET occurs when increases in the pool of

reduced CoQ ($CoQH_2$) from various metabolic pathways—in conjunction with a high proton motive force across the mitochondrial inner membrane—cause electrons to flow back through complex I instead of forward into complex III. RET can generate large amounts of mROS at complex I. We found that increased oxidation of succinate at complex II was responsible for RET mROS and that this metabolite was the source of the accumulation of $CoQH_2$. Succinate is produced in the Krebs cycle, so we investigated its metabolic source. We found that TNF increased glutamine transport into the cell, boosting glutaminolysis, which increases the pool of α-ketoglutarate supplied to the Krebs cycle, resulting in increased succinate. Mycobacteria play a critical role in TNF-induced necrosis at two distinct steps. They were required together with TNF to increase glutaminolysis and then again with the resultant mROS to induce necrosis. By contrast, TNF had no further role in the necrosis pathway beyond inducing mROS. Thus, virulent mycobacteria have evolved multiple orchestrated mechanisms to exploit host genetic vulnerabilities (i.e., dysregulated TNF levels) to mediate macrophage necrosis as a way of increasing the transmission that is critical to their survival. Delineation of the TNF-induced RET mROS pathway identified several drugs already approved for other conditions that inhibit it at different steps. These drugs also inhibited TNF-induced macrophage necrosis and the animals' hypersusceptibility to infection.

Conclusion

RET, long thought to be an in vitro artifact, is now appreciated to play important homeostatic roles through moderate increases in mROS. However, excess RET has been shown to mediate the pathology associated with ischemia–reperfusion injury in heart attack and stroke. Our work shows that RET mROS also mediates tuberculosis pathology. Paradoxically, this means that the critical host determinant TNF can go from being protective to pathogenic

depending on levels, context and the extent to which it can modulate host metabolism. Our prior work has shown that dysregulated TNF is pathogenic in human TB also. Therefore, the pathway-inhibiting drugs we have identified are promising host-targeting adjunctive drugs for tuberculosis, both drug-sensitive and drug-resistant. Metformin—a complex I inhibitor and widely used, well-tolerated anti-diabetic drug—is a particularly good candidate.

Figure 0 Caption:

Excess TNF induces pathological mROS via RET in tuberculosis. (Left) TNF induces mROS (magenta) in macrophages (green) infected with mycobacteria (blue), which causes their necrosis with exuberant growth of released mycobacteria in the debris of the tuberculosis granuloma. (**Right**) Schematic depiction of how TNF works through RIP3 and PGAM5 to elevate mROS by RET through Complex I. Metformin inhibits Complex I to prevent TNF-induced mROS.

Figure 0

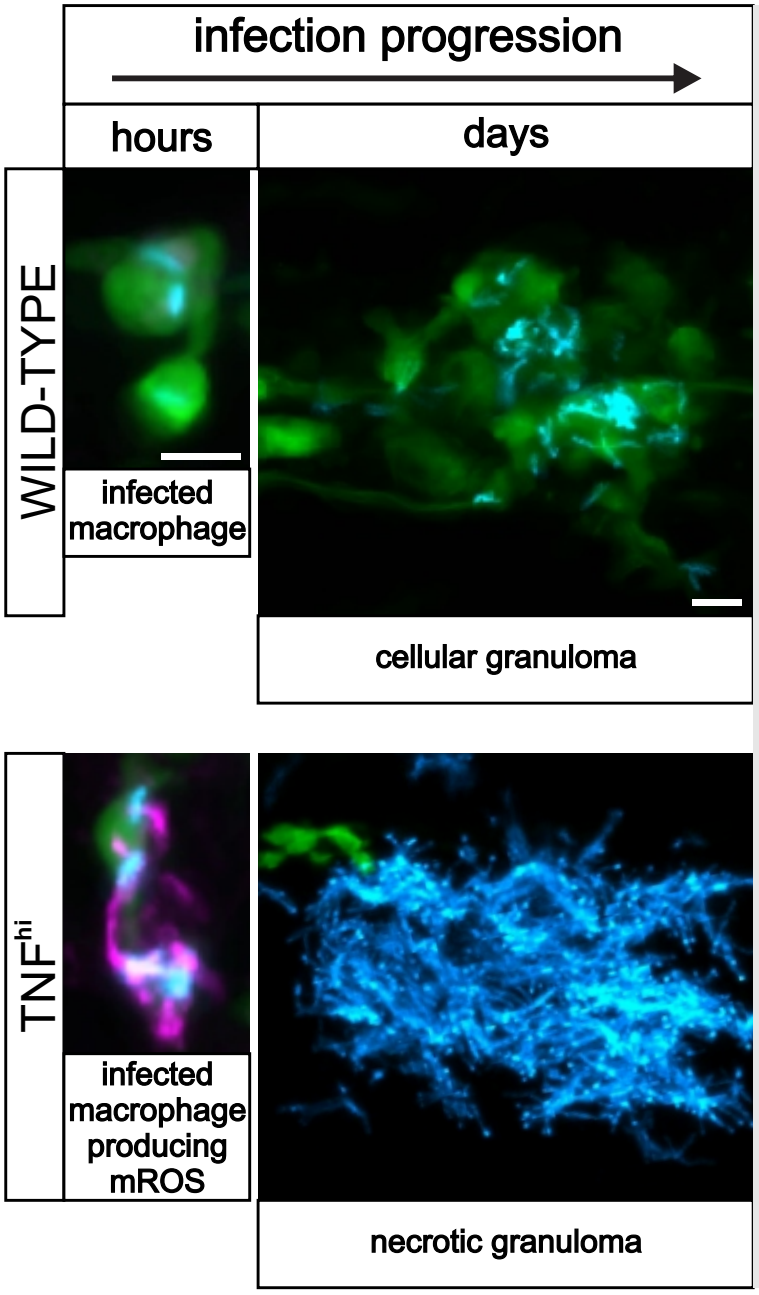
infection progression
hours
days
WILD-TYPE
infected macrophage
cellular granuloma
TNFhi
infected macrophage producing mROS
necrotic granuloma

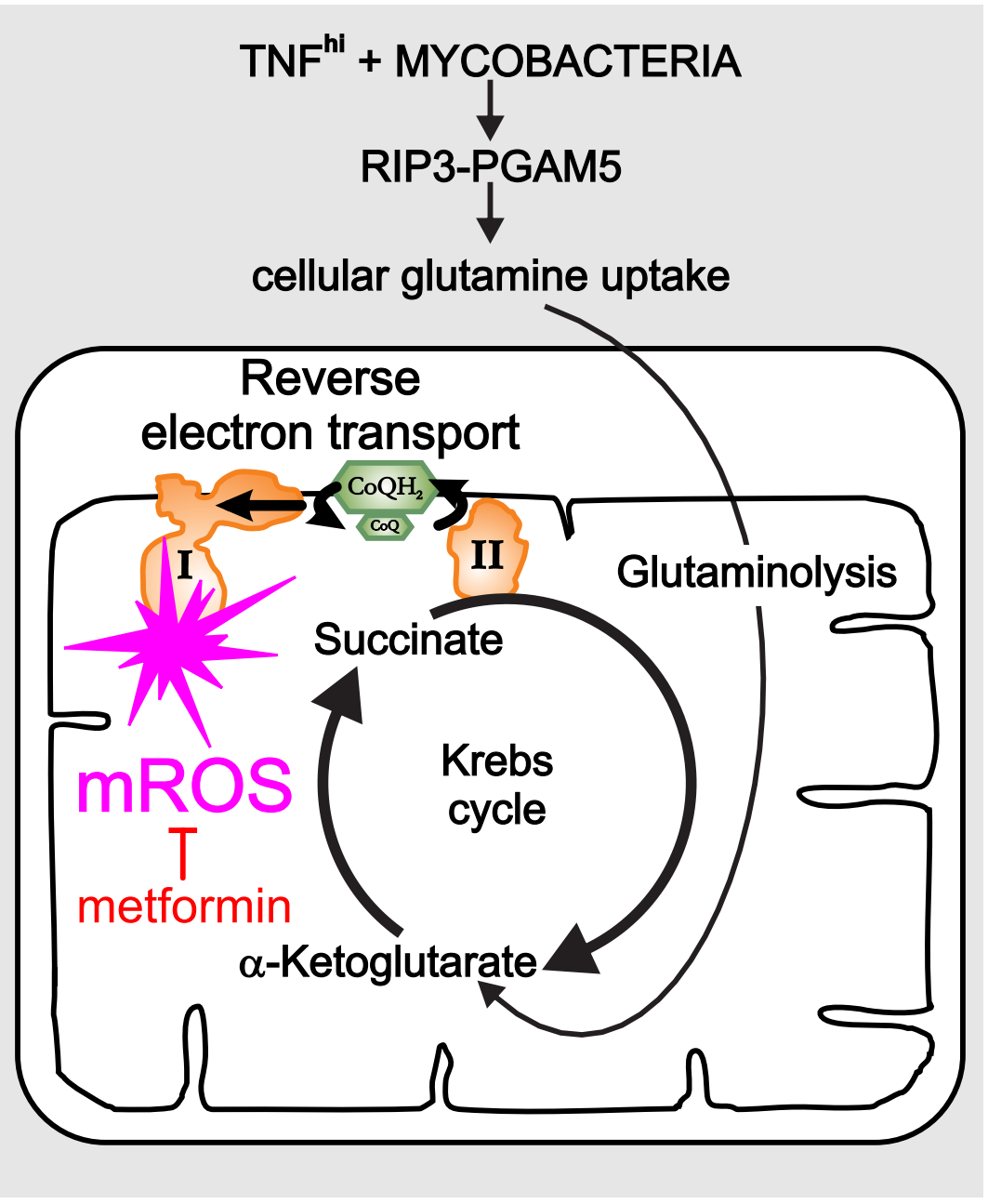
TNFhi + MYCOBACTERIA
RIP3-PGAM5
cellular glutamine uptake
Reverse electron transport
CoQH2
CoQ
I
II
Glutaminolysis
Succinate
mROS
T
metformin
Krebs cycle
α-Ketoglutarate

TNF induces pathogenic mitochondrial ROS in tuberculosis through reverse electron transport

Francisco J. Roca[1,4], Laura J. Whitworth[1,2], Hiran A. Prag[3], Michael P. Murphy[1,3] and Lalita Ramakrishnan[1,2,*]

[1] Molecular Immunity Unit, Cambridge Institute of Therapeutic Immunology and Infectious Diseases, Department of Medicine, University of Cambridge, Cambridge CB2 0AW, UK

[2] MRC Laboratory of Molecular Biology, Cambridge CB2 0QH, UK

[3] MRC Mitochondrial Biology Unit, University of Cambridge, Cambridge CB2 0XY, UK

[4] Current affiliation: Department of Biochemistry and Molecular Biology B and Immunology, Biomedical Research Institute of Murcia (IMIB-Arrixaca), University of Murcia, Murcia 30120, Spain

[*]Corresponding author: lalitar@mrc-lmb.cam.ac.uk

Abstract

Tumor necrosis factor (TNF) is a critical host resistance factor against tuberculosis. However, excess TNF produces susceptibility by increasing mitochondrial reactive oxygen species (mROS), which initiate a signaling cascade to cause pathogenic necrosis of mycobacterium-infected macrophages. Here, using the zebrafish, we identify the mechanism of TNF-induced mROS in tuberculosis. Excess TNF in mycobacterium-infected macrophages elevates mROS production by reverse electron transport (RET) through complex I. TNF-activated cellular glutamine uptake increases the Krebs cycle intermediate succinate. Oxidation of this elevated succinate by complex II drives RET, thereby generating the mROS superoxide at complex I. The complex I inhibitor, metformin, a widely used anti-diabetic drug, prevents TNF-induced mROS and necrosis of *Mycobacterium tuberculosis*-infected zebrafish and human macrophages, suggesting its utility in tuberculosis therapy.

Tumor necrosis factor (TNF) is both a host resistance and susceptibility factor in tuberculosis (TB) (*1-3*). Findings in the genetically tractable and optically transparent zebrafish larva infected with *Mycobacterium marinum* (Mm) have revealed the mechanisms behind this dual effect (*4-6*). Although TNF is required for full microbicidal activity of mycobacterium-infected macrophages, its excess causes susceptibility by inducing their necrotic death, which releases mycobacteria into the growth-permissive extracellular environment (*4, 7-9*). This pathogenic role of dysregulated TNF was revealed through a zebrafish forward genetic screen, which found that both a deficiency and excess of leukotriene A4 hydrolase (LTA4H) cause susceptibility to Mm (*4, 9*). LTA4H catalyzes the synthesis of the pro-inflammatory leukotriene B4 (LTB_4) and LTA4H/LTB_4 deficiency and excess produce TNF deficiency and excess, respectively (*4*). These zebrafish studies led to the identification of a common, functional human *LTA4H* variant associated with mortality from tuberculous meningitis, the severest form of TB (*4, 10*). In cohorts in Vietnam and Indonesia, the high LTA4H-expressing variant was associated with increased cerebrospinal fluid TNF levels and increased mortality that was mitigated by adjunctive treatment with corticosteroids, broadly acting immunosuppressants (*3, 4, 10*). These findings implicated LTB_4 and TNF-induced inflammation in mortality (*3, 4, 10*). Moreover, high TNF levels were associated with mortality even among individuals without the high LTA4H-expressing variant suggesting that TNF excess, resulting from diverse host genetic determinants, is a far-reaching host susceptibility factor in TB (*3*). Consistent with these findings, necrotic human tuberculous granulomas have more TNF than non-necrotic ones (*11*).

To gain mechanistic understanding of TNF-mediated pathogenic macrophage necrosis, we returned to the zebrafish larva. We found that excess TNF, acting through the kinase RIP3 and one of its substrates, PGAM5, increases mitochondrial reactive oxygen species (mROS) such

as superoxide and hydrogen peroxide in infected macrophages (fig. S1) (*5, 6*). These mROS activate an interorganellar signaling circuit that involves the lysosome and the endoplasmic reticulum. This ultimately causes mitochondrial calcium overload, which then leads to necrosis (fig. S1) (*5, 6*). Here, by exploiting the zebrafish larva's genetic and pharmacological tractability, we determine how TNF induces pathogenic mROS in mycobacterium-infected macrophages.

TNF induces mROS through RET

Administering exogenous TNF to Mm-infected zebrafish larvae phenocopies genetically induced TNF excess, causing macrophage necrosis and susceptibility by 5 days post-infection (fig. S2) (*4*). TNF selectively induces mROS in infected macrophages within 30 min, which rapidly trigger necrosis (*5, 6*). Using a general mitochondria-targeted ROS and oxidative stress sensor, we found that in wild-type animals, Mm infection alone causes 1.7-2.2-fold increases in mROS in infected macrophages compared to uninfected macrophages in the same animal (Fig. 1, A and B). In TNF^{hi} animals, mROS in infected macrophages were further increased to 3.6-6.6-fold over uninfected macrophages (Fig. 1, A and B). TNF did not increase mROS in uninfected macrophages, demonstrating that only infected macrophages were susceptible to TNF's effects (Fig. 1, A and B). Moreover, heat-killed Mm failed to induce mROS in both wild-type and TNF^{hi} animals, suggesting that an actively synthesized (or heat-labile) bacterial determinant is needed (Fig. 1B). To confirm that the increased TNF^{hi} mROS originated from superoxide production by the electron transport chain (ETC), we asked if it was inhibited by compounds that disrupt mitochondrial electron transport. mROS were inhibited by four compounds that disrupt mitochondrial electron transport through distinct mechanisms (Fig. 1, C to F; fig. S2; and table S1). Thus, TNF-induced mROS originate in the ETC of mycobacterium-infected macrophages.

During normal respiration, complex I receives electrons from NADH and transfers them to CoQ (Coenzyme Q), generating in the process a small amount of the mROS superoxide ($O_2^{\bullet-}$) through single electron donation to O_2 (*12*) (Fig. 2A). Increased $O_2^{\bullet-}$ production at complex I is generated by two distinct mechanisms (*12*). In the first, disruption of electron transfer, due to ETC damage or loss of cytochrome C during apoptosis, results in an accumulation of NADH derived from multiple metabolic pathways. When electrons from NADH enter complex I and cannot flow forward towards ubiquinone, they generate $O_2^{\bullet-}$ (Fig. 2A). In the second, increases in the extent of CoQ pool reduction ($CoQH_2$) from various metabolic pathways, in conjunction with a high proton motive force across the mitochondrial inner membrane, cause electrons to flow back through complex I instead of forward into complex III (Fig. 2B) (*13*). This reverse electron transport (RET) by complex I generates mROS ($O_2^{\bullet-}$ which dismutates to H_2O_2) (Fig. 2B). These two mechanisms can be distinguished by the effects of the complex I inhibitor rotenone, which increases mROS from forward electron flow through complex I but reduces mROS from RET (Fig. 2, A and B, and table S1) (*12, 14*). Rotenone increased mROS in the infected macrophages of wild-type animals, showing that they were generated by forward electron transport (Fig. 2C). By contrast, rotenone inhibited mROS in TNF^{hi} animals (Fig. 2D and table S1). Two other complex I inhibitors with different mechanisms of action also inhibited TNF^{hi} mROS (fig. S3 and table S1). Thus, TNF^{hi} mROS are generated by RET rather than by forward electron transport.

To corroborate that RET was responsible for TNF^{hi} mROS, we expressed *Ciona intestinalis* alternative oxidase (AOX) in TNF^{hi} larvae through injection of its mRNA. AOXs, which are present in plants, fungi, and some invertebrates but are absent in vertebrates, catalyze the transfer of electrons from the $CoQH_2$ pool directly to O_2, bypassing Complexes III and IV

(fig. S4A) (*15*). AOX has been shown to prevent excessive reduction of the CoQ pool and mROS increases from RET (fig. S4A) (*15*). Thus, if TNF-induced mROS are generated by RET, they should be prevented by AOX expression (*15*). We confirmed that the *C. intestinalis* AOX was active in zebrafish by showing that AOX-expressing animals were resistant to cyanide, which poisons the ETC by inhibiting complex IV (fig. S4B) (*15, 16*). AOX expression decreased TNF^{hi} mROS, consistent with generation by RET from a reduced CoQ pool (Fig. 2, B and E).

Finally, we extended these findings to *Mycobacterium tuberculosis* (Mtb), the agent of human TB, using a leucine and pantothenic acid Mtb auxotroph that can be used in containment level 2 facilities (*6*). Mtb produced similar increases in mROS as Mm (Fig. 2F). Moreover, rotenone increased mROS in wild-type macrophages and inhibited TNF-induced mROS (Fig. 2, G and H). Thus, TNF-induced mROS increases in Mtb-infected macrophages are also derived from RET.

Although there are multiple sources of increased $CoQH_2$, the most compelling candidate from both in vitro and in vivo studies was the increased oxidation of succinate at complex II (Fig. 2B) (*13, 17*). We tested this using three complex II inhibitors: atpenin A, TTFA, and dimethyl malonate (DMM), which is a prodrug of the competitive succinate dehydrogenase inhibitor malonate. All three inhibitors abolished mROS (Fig. 3A and table S1). If increased succinate oxidation at complex II was the source of RET and mROS, then increasing the mitochondrial succinate pool should have induced mROS even in wild-type animals in the absence of TNF^{hi} conditions. Diethyl succinate—a cell-permeable succinate ester known to increase mitochondrial succinate concentrations (*18*)—increased mROS in macrophages of wild-type animals (Fig. 3B). Diethyl butylmalonate (DEBM)—an inhibitor of the mitochondrial succinate transporter, which causes accumulation of endogenous mitochondrial succinate (*19*)—

performed similarly (Fig. 3B). Thus, increased oxidation of succinate at complex II is necessary and sufficient for TNF-induced RET and mROS.

TNF-activated glutaminolysis increases mitochondrial succinate

We next investigated the metabolic source of the increased succinate. Increased glycolysis, fatty acid oxidation, and glutaminolysis can all increase succinate by increasing Krebs cycle activity through increased input of pyruvate, acetyl-CoA, and α-ketoglutarate, respectively (Fig. 4A). We focused on glutaminolysis, which has been linked to TNF-mediated cell death (*20, 21*). Glutamine, the major amino acid transported in the circulation, is taken up into cells by multiple glutamine transporters and then into mitochondria where it is converted to glutamate and then α-ketoglutarate in the Krebs cycle (Fig. 4A). Four potential plasma membrane transporters that contribute to cellular glutamine uptake are highly expressed in human and zebrafish monocytes and macrophages (*22-24*). Of these, SLCA15 and SLC38A2 were identified in a screen for proteins phosphorylated by the RIP3 kinase in the context of necroptosis, a different form of TNF-mediated programmed cell death (*25*). Although distinct from necroptosis, our macrophage necrosis pathway also features RIP3, which is required for TNF-mediated mROS induction in mycobacterium-infected macrophages (fig. S1) (*5, 6*). Therefore, we tested GPNA, an inhibitor of both transporters (table S1). GPNA inhibited mROS in TNF^{hi} macrophages without affecting mROS in wild-type macrophages (Figure 4, A to C). We therefore hypothesized that TNF-RIP3-activated glutamine transport is the specific source of the increased mitochondrial glutamine for increased glutaminolysis, thereby increasing succinate. If correct, blocking the conversion of glutamine to glutamate should also specifically block TNF^{hi} mROS. Two different inhibitors of glutaminase 1 (GLS1), BPTES and CB-839 (telaglenastat), performed as expected, inhibiting mROS in TNF^{hi} but not wild-type macrophages

(Fig. 4, A to E, and table S1). By contrast, when the conversion of glutamate to α-ketoglutarate was inhibited using R-162, mROS was inhibited in both TNF^{hi} and wild-type macrophages (Fig 4, A to C, E and table S1). Thus, although the smaller increase in mROS from infection alone also requires glutaminolysis, it can be sustained by mitochondrial glutamate transported directly from the cytosol where it is produced through transamination reactions (Fig. 4, C and E). Finally, to confirm the specificity of GPNA and R-162 in our system, we used each inhibitor in combination with dimethyl glutamate, a cell permeable source of glutamate (table S1). Dimethyl glutamate restored GPNA-inhibited mROS but not R-162-inhibited mROS (Fig. 4F). Thus, TNF stimulation of infected macrophages specifically activates glutamine uptake to increase glutaminolysis to induce mROS.

If high TNF also increases glycolysis and/or fatty acid oxidation (Fig. 4A), then inhibiting these pathways should also specifically inhibit TNF^{hi} but not wild-type mROS. However, inhibition of mitochondrial pyruvate transport using UK5099, or fatty acid oxidation using perhexiline or 4-bromocrotonic acid (4-BrCA) removed mROS in both wild-type and TNF^{hi} animals (Fig. 4, G to I, and table S1). We confirmed the specificity of UK5099 and perhexiline by showing that methyl pyruvate, a cell-permeable pyruvate derivative restored mROS inhibited by them but not by GPNA or R-162 (Fig. 4, J and K). Thus, TNF and infection together activate cellular glutamine uptake and the resultant increase in glutaminolysis is the specific source of the increased succinate. Because oxidation of excess succinate would increase the levels of the downstream intermediates malate and oxaloacetate (a potent complex II inhibitor) (*26*), glycolysis and fatty acid oxidation would be required to play a "supporting role" by providing acetyl-CoA to consume oxaloacetate. Thus, the build-up of oxaloacetate would be prevented, allowing continued complex II activity (Fig. 4A).

We used liquid chromatography–mass spectrometry to quantify succinate levels in the larvae under the different conditions. Infection and TNF combined (but neither alone) increased succinate levels over baseline (Fig. 5A and data S1). Moreover, GPNA and BPTES inhibited this increase, as predicted (Fig. 5A and data S1). Although further validation of the source of succinate by measurement of flux to it from stable isotope labeled precursors such as glutamine was not technically possible in this in vivo system, our findings that both mROS and succinate levels increase in the TNF^{hi} state and decrease to wild-type levels upon inhibiting glutamine uptake or its conversion to glutamate provide strong evidence that glutaminolysis from increased glutamine transport is the source of the increased succinate. As with mROS increases, these succinate increases also occurred rapidly within 30 min of TNF administration. The rapid induction of succinate and mROS is consistent with TNF–RIP3-induced post-translational modifications (e.g., phosphorylation), as previously proposed (*20, 21*). Accordingly, RIP3 knockdown inhibited TNF-induced succinate in infected animals (Fig. 5B and data S1). Finally, TNF-induced succinate was also inhibited by knockdown of PGAM5, a mitochondrial phosphatase, which is required together with RIP3 both for TNF-mediated necroptosis (*27*) and for TNF-induced mROS and necrosis of mycobacterium-infected macrophages in our pathway (Fig. 5B, data S1 and fig. S1) (*5, 6*). Thus, TNF signals via RIP3 and PGAM5 to activate glutamine transport to increase glutaminolysis and Krebs cycle succinate.

TNF, mROS, and mycobacteria play discrete roles in macrophage necrosis

We dissected the interactions between TNF, mROS, and mycobacteria and what roles they play at distinct steps of the pathway. We had shown that both TNF and mycobacteria are required to increase mitochondrial succinate, which is required to induce mROS. Because exogenous succinate could induce mROS in wild-type animals in both infected and uninfected

174 macrophages (Fig. 3B), we concluded that the only role for TNF and mycobacteria in mROS
175 induction in this system is to increase mitochondrial succinate.
176 We have previously shown that the mROS are required for macrophage necrosis (*5*). We
177 now asked whether they were sufficient to complete macrophage necrosis or whether TNF
178 and/or mycobacteria further required downstream of mROS induction. Macrophage necrosis
179 results in exuberant extracellular mycobacterial growth in characteristic cords (Fig. 6A).
180 Bacterial cording can be used as a reliable surrogate marker for infected macrophage death (*9*).
181 We found that both exogenous succinate and DEBM induced the necrosis of infected
182 macrophages as evidenced by increased bacterial cording (Fig. 6B). This necrosis was a direct
183 consequence of RET mROS production, as disrupting the ETC with diazoxide reduced cording
184 (Fig. 6B). Moreover, bypassing the ETC by AOX expression—which decreased TNF-induced
185 mROS (Fig 2E)—inhibited both TNF-mediated macrophage necrosis (Fig 6C) as well as
186 succinate- and DEBM-induced necrosis in wild-type animals (Fig. 6D). Thus, TNF plays no
187 further role in macrophage necrosis beyond increasing mitochondrial succinate.
188 To determine if mycobacteria were required for necrosis downstream of mROS
189 induction, we examined if diethyl succinate and DEBM could also kill uninfected macrophages
190 by enumerating macrophages in infected and uninfected animals (*5*). Diethyl succinate and
191 DEBM reduced macrophage numbers only in the infected animals, suggesting that, in contrast to
192 TNF, mycobacteria are required downstream of mROS to induce necrosis (Fig. 6E).
193 Similar results were observed in human macrophages derived from the monocytic cell
194 line THP-1. We had previously shown that TNF induces necrosis in Mtb-infected THP-1 cells
195 through the same interorganellar pathway downstream of mROS as in Mm-infected zebrafish
196 (fig. S2) (*6*). We used rotenone to confirm that RET was responsible for mROS induction in

these cells. In the absence of TNF, rotenone increased death of both infected and uninfected cells, as expected from the oxidative stress it induces, but there was a specific reduction of TNF-induced death of infected macrophages (Fig. 6F). Next, to test our findings from zebrafish concerning about the role of TNF, mROS, and mycobacteria, we treated Mtb-infected THP-1 cells with MitoParaquat (MitoPQ), a mitochondria-targeted compound that produces superoxide through redox cycling at the complex I flavin site (table S1). MitoPQ increased necrosis in the absence of TNF but only in infected macrophages (Fig. 6G and fig. S2). This confirmed that TNF has no further role in the necrosis pathway beyond inducing mROS whereas mycobacteria are required downstream of mROS induction. By contrast, one or more mycobacterial factors shared between Mm and Mtb operate at two distinct points in this pathway: first to enable TNF-mediated mROS by activating cellular glutamine uptake and increasing mitochondrial succinate to produce complex II-mediated RET-ROS and then to promote the necrosis of macrophages experiencing this mROS (Fig. 6H).

mROS pathway reveals host-targeting drugs for TB

We had previously shown that blocking mROS using scavengers such as N-acetyl cysteine inhibited TNF-induced macrophage necrosis and restored resistance (*5*). Four of the compounds used here to inhibit mROS, and thus delineate the mechanism of mROS production, are approved oral drugs or under investigation for other conditions. We therefore assessed if these drugs also inhibited macrophage necrosis (fig. S5). These included diazoxide, a disruptor of electron transport that is approved for hyperinsulinemic hypoglycemia; perhexiline, a mitochondrial carnitine palmitoyltransferase-1 inhibitor that is approved for angina; telaglenastat, a GLS1 inhibitor that is in clinical trials for cancer; and DMM, the complex II inhibitor that has been shown to prevent ischemia-reperfusion injury in models of heart attack

(fig. S5 and table S1) (*28*). All four inhibited TNF-mediated macrophage necrosis in the zebrafish (Figure 7, A to E). We then asked if metformin, a widely-used antidiabetic drug that inhibits Complex I (fig. S5 and table S1) (*29*), could be a potential host-targeting drug to prevent TNF-induced pathogenic macrophage necrosis in TB. Metformin inhibited TNF-elicited mROS in Mm-infected larvae as did its more hydrophobic derivative phenformin (Fig. 7F). Metformin also inhibited TNF-mediated necrosis of Mm-infected macrophages (Fig. 7G). Moreover, it also inhibited Mm-infected macrophage necrosis resulting from increased mitochondrial succinate (Fig. 7H). Thus, although metformin has pleiotropic effects and is a relatively weak complex I inhibitor (*29*), it specifically inhibits TNF-mediated necrosis by blocking RET-generated mROS at Complex I. Finally, metformin inhibited mROS in the infected macrophages of Mtb-infected zebrafish (Fig. 7I) and inhibited necrosis of Mtb-infected THP-1 cells (Fig. 7J), confirming that its inhibitory activity was relevant in the context of Mtb infection.

DISCUSSION

Though long thought to be an in vitro artifact, moderate levels of RET and resultant increases in mROS have important homeostatic roles in cell differentiation and oxygen sensing (*13*). However, excess RET has pathological roles in ischemia–reperfusion injury of the heart and brain (*18, 30*). During ischemia, rewiring of the Krebs cycle reduces fumarate levels, leading to succinate accumulation (*18*). During the reperfusion phase, rapid oxidation of the accumulated succinate triggers RET and mROS, which causes tissue necrosis leading to irreparable organ damage (*18, 30*). The TNF-mediated necrosis pathway described here has two significant differences. First, the source of the succinate is different and second, in ischemia–reperfusion injury, the mROS alone appear sufficient to drive necrosis whereas a second “hit” in the form of one or more bacterial determinants is required in our TNF-induced macrophage necrosis

pathway. Perhaps the inflammatory milieu generated during ischemia generates the additional signal(s) that combine with mROS to cause necrosis.

We also considered our findings in the light of work using cultured macrophages, which has shown that succinate is responsible for generating proinflammatory responses to lipopolysaccharide (LPS), a key virulence determinant of Gram-negative bacteria (*19*). LPS causes macrophages to switch to aerobic glycolysis while generating succinate from enhanced glutaminolysis by an undescribed means. Succinate induces mROS, likely through RET, and these mROS drive pro-inflammatory cytokines via HIF1α stabilization (*19*, *31*). This sequence contrasts with the pathway described here where TNF is upstream, not downstream, of mROS and TNF is not among the cytokines induced by LPS and succinate. Thus, distinct pathogenic determinants specific to Gram-negative bacteria and mycobacteria—a cell wall constituent versus a product of live mycobacteria—channel mROS to produce discrete cellular responses.

We were particularly interested in pursuing this TNF-mediated necrosis pathway because of its clinical implications. Currently, tuberculous meningitis is treated with adjunctive corticosteroids which are broadly immunosuppressive and have multiple additional serious adverse effects. Our prior studies on the TNF-mediated necrosis pathway identified several pathway-specific drugs that inhibit macrophage necrosis without being broadly anti-inflammatory, all with a decades-long history of use in humans for other conditions (*5*, *6*). This work now identifies additional drugs, including the widely used oral antidiabetic drug, metformin. Metformin readily crosses the blood-brain barrier, resulting in high brain and CSF concentrations (table S1) (*32*). This highlights its potential therapeutic utility in tuberculous meningitis. Metformin was reported to ameliorate Mtb infection in mice via diverse mechanisms, including broadly acting anti-inflammatory effects and to enhance the efficacy of antitubercular

antibiotics in one but not another study, leading to an ongoing trial as an adjunctive agent for lung TB (*33-36*). Adjunctive corticosteroid treatment has been suggested to reduce inflammation and bacterial burdens in lung TB, the most common, contagious form that sustains the global disease burden (*37*, *38*). It will be interesting to see whether metformin particularly benefits individuals with the high *LTA4H* genotype, and, given the association of TNF with necrotic lung granulomas (*11*), whether it has a particular benefit in resolving necrotic lesions.

MATERIALS AND METHODS

Zebrafish husbandry and infections

Zebrafish husbandry and experiments were conducted in compliance with guidelines from the UK Home Office using protocols approved by the Animal Welfare and Ethical Review Body of the University of Cambridge. Zebrafish AB wild-type strain (Zebrafish International Resource Center) (ZFIN ID: ZDB-GENO-960809-7) and the transgenic line *Tg(mpeg1:YFP)*^{w200} (with yellow fluorescent macrophages) (ZFIN ID: ZDB-FISH-150901-6828) (*6*) in the AB background were used. All zebrafish lines were maintained in buffered reverse osmotic water systems as previously described (*6*). Zebrafish embryos were housed at 28.5°C in fish water from collection to 1 day post-fertilization (dpf) and in E2 Embryo Medium diluted to 0.5X (E2/2) supplemented with 0.003% 1-phenyl-2-thiourea (PTU) (Sigma) from 1 dpf to prevent pigmentation (*6*). Larvae (of undetermined sex given the early developmental stages used) were anesthetized, infected at 2 dpf via caudal vein (CV) injection for all assays, and randomly allotted to the different experimental conditions as previously described (*6*, *59*). Sample size was determined based on previous similar experiments or on pilot experiments.

Bacterial strains

289 Mm M strain (ATCC #BAA-535) and Mtb H37Rv strain, mc^{2}6206 *ΔleuD ΔpanCD* (*60*)
290 expressing tdTomato, mWasabi, or EBFP2 were grown as previously described (*59, 61*). For
291 experiments to assay bacterial cording and number of macrophages in the trunk of the animal,
292 zebrafish larvae were infected with 150-200 tdTomato-expressing Mm. To assess mROS, larvae
293 were infected with 90-120 EBFP2-expressing or 84 mWasabi-expressing Mm, 80-100 EBFP2-
294 expressing Mtb, or injected with 336 heat-killed mWasabi-expressing Mm (heat-killed by
295 incubation at 80°C for 20 min). To assess succinate levels, zebrafish larvae were infected with
296 200-300 tdTomato-expressing Mm.
297 TNF and drug administration to zebrafish larvae
298 TNF^{hi} animals were created by injecting recombinant zebrafish soluble TNF (*62*) as
299 previously described (*4*). To assess drug treatment in infected fish, equivalently infected sibling
300 larvae were mixed in a Petri dish and held at 28.5°C before random allocation to the drug-treated
301 or control groups; 0.5% DMSO (Sigma) was used as the control (vehicle). Drugs dissolved in
302 DMSO or water were kept in small aliquots at −20°C before administration to 1 dpi larvae by
303 adding them to the water (E2/2 medium). Doses used in this work were based on previous
304 studies or pilot experiments, using the minimum effective concentration without deleterious or
305 toxic effects on larvae for the duration of the experiment (see table S2). FCCP (carbonyl
306 cyanide-4-(trifluoromethoxy)phenylhydrazone) (50 nM) (Cambridge Bioscience) was
307 administered 1.5 hours before MitoTracker Red CM-H_2-Xros injection. TTFA
308 (thenoyltrifluoroacetone) (1 μM) (Cambridge Bioscience), atpenin A5 (2.5 nM) (Insight
309 Biotechnology), diethyl succinate (500 nM) (reagent plus 99% Sigma), and DEBM (diethyl butyl
310 malonate) (1 μM) (Sigma) were administered 2 hours before MitoTracker Red CM-H_2-Xros
311 injection. DM-Glutamate (dimethyl glutamate) (60 μM) (Cambridge Bioscience) was

administered 3 hours before MitoTracker Red CM-H_2-Xros injection. DNP (2.4-dinitrophenol) (100 nM) (Agilent Technologies) was administered 3.5 hours before MitoTracker Red CM-H_2-Xros injection. Rotenone (6.25 nM) (Sigma), piericidin A (50 nM) (Stratech Scientific), strobilurin B (100nM) (Insight Biotechnology), metformin (20 μM) (VWR International), phenformin (20 μM) (Sigma), nigericin (5 μM) (Sigma), diazoxide (50 nM) (Cambridge Bioscience), UK5099 (10 μM) (Cambridge Bioscience), and M-pyruvate (methyl pyruvate) (50 nM) (Fisher Scientific) were administered 4 hours before MitoTracker Red CM-H_2-Xros injection. DM-malonate (dimethyl malonate) (10 μM) (Sigma), perhexiline (10 μM) (Stratech Scientific), 4-BrCA (4-bromocrotonic acid) (10 μM) (Insight Biotechnology), GPNA (10 μM) (Cambridge Bioscience), BPTES (5 μM) (Cambridge Bioscience), telaglenastat (5 μM) (Cambridge Bioscience), and R-162 (1 μM) (Cambridge Bioscience) were administered 5 hours before MitoTracker Red CM-H_2-Xros injection. In experiments to assess cording, perhexiline was removed 5 hours after TNF administration, diethyl succinate and DEBM were administered for 10 hours and then removed, and metformin, phenformin, DM-malonate, diazoxide, and telaglenastat were added 1 dpi and removed 2 dpi. After drug removal, the larvae were maintained in fresh E2/2 medium for the rest of the experiment. In experiments to assess macrophage numbers, diethyl succinate and DEBM were administered 1 dpi for 24 hours until macrophage number was assessed 2 dpi. For experiments quantifying mitochondrial ROS production, drugs were added before MitoTracker Red CM-H_2-Xros injection as indicated above and maintained during imaging.

Synthetic mRNA synthesis and microinjection

The ORF sequence of the alternative oxidase (AOX) from *Ciona intestinalis* was obtained by PCR using as a template the plasmid MAC_C_AOX (Addgene plasmid# 111661).

The T7 promoter (5′-TAATACGACTCACTATAGG-3′) followed by the zebrafish Kozak sequence 5′-GCCGCCACC-3′ were inserted before the start codon by PCR. mRNA was synthesized using the mMessage mMachine kit (Ambion) and the polyA Tailing kit (Ambion). Approximately 2-4 nl of injection solution (*4*) containing 200 μg/ml of AOX mRNA was injected into the yolks of embryos at the one-to-two-cell stage.

Morpholino-mediated knockdown of RIP3 and PGAM5

RIP3 e2/i2-splice-blocking (5′-TTTTAGAAATCACCTTGGCATCCAG-3′) and PGAM5-translation-blocking morpholino (5′-AGCGCCCTCCGAAAAGACATGCTTC-3′) (Gene Tools) were diluted to 0.15 mM in injection solution (*4*). Approximately 2-4 nl was injected into the yolks of embryos at the one-to-two-cell stage.

Heart rate assessment of zebrafish larvae

AOX-expressing 2 dpf larvae were treated with different concentrations of KCN for an hour. Heart rate (beats per minute) was assessed as a readout of cyanide poisoning of complex IV of the electron transport chain (*63*) in absence of anesthetic using a dissecting microscope.

Zebrafish larvae microscopy

Fluorescence microscopy was performed as described (*59*). Mycobacterial cording and macrophage numbers were assessed in the trunk of the larvae using a Nikon Eclipse E600 upright microscope fitted with Nikon Plan Fluor 10X 0.3 NA and Nikon Plan Fluor 20X 0.5 NA objectives. For laser scanning confocal microscopy, anesthetized larvae were embedded in low-melting-point agarose as previously described (*6*). A Nikon A1R confocal microscope with a Plan Apo 20X 0.75 NA objective was used to generate 35-40 mm *z*-stacks consisting of 0.3-2-mm optical sections. The galvano scanner was used for all static imaging and for time-lapse imaging of the caudal hematopoietic tissue (CHT, area located between the cloaca and the

beginning of the caudal fin). Images were acquired with NIS Elements (Nikon). A heating chamber (Oko-labs) adapted to the microscope was used to maintain temperature at 28.5°C during imaging. Confocal images are pseudocolored to facilitate visualization.

Mitochondrial ROS quantification assay in zebrafish larvae

Mitochondrial ROS production was assayed by fluorescence intensity of MitoTracker Red CM-H_2-Xros, a cell-permeable fluorogenic probe for ROS which is targeted to the mitochondrion and produces red fluorescence upon oxidation by diverse ROS (Fisher Scientific) (*5, 6*). *Tg(mpeg1:YFP)*^{w200} larvae were infected 2 dpf. For all experiments where TNF^{hi} animals are used, larvae were microinjected 1 dpi via CV with phosphate buffered saline (PBS) containing TNF and 50 mM MitoTracker Red CM-H_2-Xros or PBS containing vehicle for TNF and MitoTracker Red CM-H_2-Xros (*6*). For experiments where mROS production was quantified in mycobacterium-infected versus uninfected macrophages, 100 mM MitoTracker Red CM-H_2-Xros was used instead to increase sensitivity of the probe. After administration of MitoTracker Red CM-H_2-Xros (in combination with TNF or alone), larvae were prepared for confocal imaging and maintained at 28.5°C within a heated incubation chamber attached to the confocal microscope. Images of the CHT of each larva were taken starting 30-60 min after MitoTracker Red CM-H_2-Xros administration. Mitochondrial ROS production was quantified using maximum projection images as MitoTracker Red CM-H_2-Xros maximum fluorescence intensity per macrophage using NIS-Elements. When not otherwise stated in the figure legend, the mean of maximum MitoTracker Red CM-H_2-Xros fluorescence was quantified only in Mm- or Mtb-infected macrophages.

Succinate quantification by liquid chromatography-mass spectrometry

Three to six pools of 20 1-dpi larvae per condition per experiment were collected and flash frozen 30 min after TNF injection, with the time set after injecting 75% of the larvae for each experimental group. Each pool was homogenized in 300 µl of extraction buffer and succinate was quantified as described (*64*). The means and pooled standard deviations of independent experiments were calculated and compared using one-way ANOVA with Tukey's post-hoc multiple comparisons test.

Quantification of THP-1 cell necrosis

THP-1 cells (ATCC TIB-202) were differentiated into macrophages and infected with single-cell suspensions of mCherry- or tdTomato-expressing Mtb mc^{2}6206 *ΔleuD ΔpanCD* as described (*6*). In THP-1 experiments with added TNF, 1-day post-infection cells were pre-incubated with 10 nM rotenone, 1 mM metformin or 0.1% DMSO vehicle control for 1 hour. Human recombinant TNF (Sigma) in a solution of 5% trehalose/PBS (Sigma) was then added to treatment wells as described (*6*). In the experiment with 5 µM mitoparaquat, drug or 0.1% DMSO vehicle control was added 1 day post Mtb infection and images acquired after 5 hours incubation. SYTOX® Green Nucleic Acid Stain (Life Technologies) was added to culture medium 30 min before image acquisition. Macrophages were imaged using a Nikon Ti-E inverted microscope fitted with a 20X objective (Nikon, CFI S Plan Fluor 0.45 NA) and 2-5 arbitrary images per well acquired with NIS Elements (Nikon). Cell necrosis was quantified using a previously described method (*6*).

Statistical analysis

The following statistical analyses were performed using Prism 7 (GraphPad): two-way ANOVA or one-way ANOVA with Dunn's or Tukey's post-test and Fisher's exact test. Error bars represent the standard error of mean. Post-test *P*-values were defined as follows: Not

significant, $P>0.05$; *$P<0.05$; ** $P<0.01$; ***$P<0.001$; and ****$P<0.0001$. The statistical tests used for each figure can be found in the corresponding figure legend. Where the *n* value is given and not represented graphically in the figure, *n* represents the number of zebrafish used for each experimental group.

Software used

The following software was used: NIS-Elements for image acquisition in wide-field and confocal microscopy, ImageJ (https://fiji.sc/) for image analysis of macrophage death, GraphPad Prism 7.0 (GraphPad Software, Inc., San Diego, CA) for data graphing and statistical analyses, and CorelDRAW (CorelDRAW Graphics Suite x5) for figure preparation.

References and Notes:

1. J. Keane et al., Tuberculosis associated with infliximab, a tumor necrosis factor alpha-neutralizing agent. N Engl J Med 345, 1098-1104 (2001).

2. M. A. Behr, P. H. Edelstein, L. Ramakrishnan, Is Mycobacterium tuberculosis infection life long? BMJ 367, l5770 (2019).

3. L. J. Whitworth et al., Elevated cerebrospinal fluid cytokine levels in tuberculous meningitis predict survival in response to dexamethasone. PNAS 118(10):e2024852118. doi: 10.1073/pnas.2024852118 (2021).

4. D. M. Tobin et al., Host genotype-specific therapies can optimize the inflammatory response to mycobacterial infections. Cell 148, 434-446 (2012).

5. F. J. Roca, L. Ramakrishnan, TNF dually mediates resistance and susceptibility to mycobacteria via mitochondrial reactive oxygen species. Cell 153, 521-534 (2013).

6. F. J. Roca, L. J. Whitworth, S. Redmond, A. A. Jones, L. Ramakrishnan, TNF Induces Pathogenic Programmed Macrophage Necrosis in Tuberculosis through a Mitochondrial-Lysosomal-Endoplasmic Reticulum Circuit. Cell 178, 1344-1361 e1311 (2019).

7. C. J. Cambier, S. Falkow, L. Ramakrishnan, Host evasion and exploitation schemes of Mycobacterium tuberculosis. Cell 159, 1497-1509 (2014).

8. H. Clay, H. E. Volkman, L. Ramakrishnan, Tumor necrosis factor signaling mediates resistance to mycobacteria by inhibiting bacterial growth and macrophage death. Immunity 29, 283-294 (2008).

9. D. M. Tobin et al., The lta4h locus modulates susceptibility to mycobacterial infection in zebrafish and humans. Cell 140, 717-730 (2010).

10. L. Whitworth et al., A Bayesian analysis of the association between Leukotriene A4 Hydrolase genotype and survival in tuberculous meningitis. Elife 10:e61722. doi: 10.7554/eLife.61722 (2021).

11. M. J. Marakalala et al., Inflammatory signaling in human tuberculosis granulomas is spatially organized. Nat Med 22, 531-538 (2016).

12. M. P. Murphy, How mitochondria produce reactive oxygen species. Biochem J 417, 1-13 (2009).

13. F. Scialo, D. J. Fernandez-Ayala, A. Sanz, Role of Mitochondrial Reverse Electron Transport in ROS Signaling: Potential Roles in Health and Disease. Front Physiol 8, 428 (2017).

14. R. Fato et al., Differential effects of mitochondrial Complex I inhibitors on production of reactive oxygen species. Biochim Biophys Acta 1787, 384-392 (2009).

15. E. L. Robb et al., Control of mitochondrial superoxide production by reverse electron transport at complex I. J Biol Chem 293, 9869-9879 (2018).

16. H. Nuskova, M. Vrbacky, Z. Drahota, J. Houstek, Cyanide inhibition and pyruvate-induced recovery of cytochrome c oxidase. J Bioenerg Biomembr 42, 395-403 (2010).

17. N. Burger et al., A sensitive mass spectrometric assay for mitochondrial CoQ pool redox state in vivo. Free Radic Biol Med 147, 37-47 (2020).

18. E. T. Chouchani et al., Ischaemic accumulation of succinate controls reperfusion injury through mitochondrial ROS. Nature 515, 431-435 (2014).

19. E. L. Mills et al., Succinate Dehydrogenase Supports Metabolic Repurposing of Mitochondria to Drive Inflammatory Macrophages. Cell 167, 457-470 e413 (2016).

20. D. W. Zhang et al., RIP3, an energy metabolism regulator that switches TNF-induced cell death from apoptosis to necrosis. Science 325, 332-336 (2009).

21. V. Goossens, G. Stange, K. Moens, D. Pipeleers, J. Grooten, Regulation of tumor necrosis factor-induced, mitochondria- and reactive oxygen species-dependent cell death by the electron flux through the electron transport chain complex I. Antioxid Redox Signal 1, 285-295 (1999).

22. https://www.proteinatlas.org/

23. A. Broer, F. Rahimi, S. Broer, Deletion of Amino Acid Transporter ASCT2 (SLC1A5) Reveals an Essential Role for Transporters SNAT1 (SLC38A1) and SNAT2 (SLC38A2) to Sustain Glutaminolysis in Cancer Cells. J Biol Chem 291, 13194-13205 (2016).

24. https://www.sanger.ac.uk/tool/basicz/

25. C. Q. Zhong et al., Quantitative phosphoproteomic analysis of RIP3-dependent protein phosphorylation in the course of TNF-induced necroptosis. Proteomics 14, 713-724 (2014).

26. A. Stepanova, Y. Shurubor, F. Valsecchi, G. Manfredi, A. Galkin, Differential susceptibility of mitochondrial complex II to inhibition by oxaloacetate in brain and heart. Biochim Biophys Acta 1857, 1561-1568 (2016).

27. Z. Wang, H. Jiang, S. Chen, F. Du, X. Wang, The mitochondrial phosphatase PGAM5 functions at the convergence point of multiple necrotic death pathways. Cell 148, 228-243 (2012).

28. H. A. Prag et al., Ester Prodrugs of Malonate with Enhanced Intracellular Delivery Protect Against Cardiac Ischemia-Reperfusion Injury In Vivo. Cardiovasc Drugs Ther, 1:1-13. doi: 10.1007/s10557-020-07033-6 (2020).

29. G. Vial, D. Detaille, B. Guigas, Role of Mitochondria in the Mechanism(s) of Action of Metformin. Front Endocrinol (Lausanne) 10, 294 (2019).

30. A. Stepanova et al., Reverse electron transfer results in a loss of flavin from mitochondrial complex I: Potential mechanism for brain ischemia reperfusion injury. J Cereb Blood Flow Metab 37, 3649-3658 (2017).

31. G. M. Tannahill et al., Succinate is an inflammatory signal that induces IL-1β through HIF-1α. Nature 496, 238-242 (2013).

32. K. Łabuzek et al., Quantification of metformin by the HPLC method in brain regions, cerebrospinal fluid and plasma of rats treated with lipopolysaccharide. Pharmacol Rep 62, 956-965 (2010).

33. A. Singhal et al., Metformin as adjunct antituberculosis therapy. Sci Transl Med 6, 263ra159 (2014).

34. L. Tsenova, A. Singhal, Effects of host-directed therapies on the pathology of tuberculosis. J Pathol 250, 636-646 (2020).

35. C. Padmapriyadarsini et al., Evaluation of metformin in combination with rifampicin containing antituberculosis therapy in patients with new, smear-positive pulmonary tuberculosis (METRIF): study protocol for a randomised clinical trial. BMJ Open 9, e024363 (2019).

36. N. K. Dutta, M. L. Pinn, P. C. Karakousis, Metformin Adjunctive Therapy Does Not Improve the Sterilizing Activity of the First-Line Antitubercular Regimen in Mice. Antimicrob Agents Chemother 61, (2017).

37. P. Muthuswamy, T. C. Hu, B. Carasso, M. Antonio, N. Dandamudi, Prednisone as adjunctive therapy in the management of pulmonary tuberculosis. Report of 12 cases and review of the literature. Chest 107, 1621-1630 (1995).

38. R. A. Smego, N. Ahmed, A systematic review of the adjunctive use of systemic corticosteroids for pulmonary tuberculosis. Int J Tuberc Lung Dis 7, 208-213 (2003).

39. Rotenone as an Insecticide. Nature 132, 167-167 (1933).

40. H. Balba, Review of strobilurin fungicide chemicals. Journal of Environmental Science and Health, Part B 42, 441-451 (2007).

41. R. Yendapally et al., A review of phenformin, metformin, and imeglimin. Drug Dev Res 81, 390-401 (2020).

42. I. Pernicova, M. Korbonits, Metformin--mode of action and clinical implications for diabetes and cancer. Nat Rev Endocrinol 10, 143-156 (2014).

43. R. D. Guzy, B. Sharma, E. Bell, N. S. Chandel, P. T. Schumacker, Loss of the SdhB, but Not the SdhA, subunit of complex II triggers reactive oxygen species-dependent hypoxia-inducible factor activation and tumorigenesis. Mol Cell Biol 28, 718-731 (2008).

44. S. Drose, Differential effects of complex II on mitochondrial ROS production and their relation to cardioprotective pre- and postconditioning. Biochim Biophys Acta 1827, 578-587 (2013).

45. S. Cadenas, Mitochondrial uncoupling, ROS generation and cardioprotection. Biochim Biophys Acta Bioenerg 1859, 940-950 (2018).

46. J. Li et al., Mechanism of the hypoxia inducible factor 1/hypoxic response element pathway in rat myocardial ischemia/diazoxide postconditioning. Mol Med Rep 21, 1527-1536 (2020).

47. J. Black, Diazoxide and the treatment of hypoglycemia: an historical review. Ann N Y Acad Sci 150, 194-203 (1968).

48. Z. Yang et al., RIP3 targets pyruvate dehydrogenase complex to increase aerobic respiration in TNF-induced necroptosis. Nat Cell Biol 20, 186-197 (2018).

49. A. Steggall, I. R. Mordi, C. C. Lang, Targeting Metabolic Modulation and Mitochondrial Dysfunction in the Treatment of Heart Failure. Diseases 5, (2017).

50. B. C. Sallustio, I. S. Westley, R. G. Morris, Pharmacokinetics of the antianginal agent perhexiline: relationship between metabolic ratio and steady-state dose. Br J Clin Pharmacol 54, 107-114 (2002).

51. M. S. Padanad et al., Fatty Acid Oxidation Mediated by Acyl-CoA Synthetase Long Chain 3 Is Required for Mutant KRAS Lung Tumorigenesis. Cell Rep 16, 1614-1628 (2016).

52. L. Yang, S. Venneti, D. Nagrath, Glutaminolysis: A Hallmark of Cancer Metabolism. Annu Rev Biomed Eng 19, 163-194 (2017).

53. https://clinicaltrials.gov/ct2/show/NCT02071862

54. L. Jin, G. N. Alesi, S. Kang, Glutaminolysis as a target for cancer therapy. Oncogene 35, 3619-3625 (2016).

55. A. Rossi et al., Defective Mitochondrial Pyruvate Flux Affects Cell Bioenergetics in Alzheimer's Disease-Related Models. Cell Rep 30, 2332-2348 e2310 (2020).

56. M. Casimir et al., Mitochondrial glutamate carrier GC1 as a newly identified player in the control of glucose-stimulated insulin secretion. J Biol Chem 284, 25004-25014 (2009).

57. E. L. Robb et al., Selective superoxide generation within mitochondria by the targeted redox cycler MitoParaquat. Free Radic Biol Med 89, 883-894 (2015).

58. https://www.epa.gov/ingredients-used-pesticide-products/paraquat-dichloride

59. K. Takaki, J. M. Davis, K. Winglee, L. Ramakrishnan, Evaluation of the pathogenesis and treatment of Mycobacterium marinum infection in zebrafish. Nat Protoc 8, 1114-1124 (2013).

60. J. M. Mouton et al., Comprehensive Characterization of the Attenuated Double Auxotroph Mycobacterium tuberculosisΔleuDΔpanCD as an Alternative to H37Rv. Frontiers in Microbiology 10:1922. doi: 10.3389/fmicb.2019.01922 (2019).

61. M. M. Osman et al., The C terminus of the mycobacterium ESX-1 secretion system substrate ESAT-6 is required for phagosomal membrane damage and virulence. Proc Natl Acad Sci U S A 119, e2122161119 (2022).

62. F. J. Roca et al., Evolution of the inflammatory response in vertebrates: fish TNF-alpha is a powerful activator of endothelial cells but hardly activates phagocytes. J Immunol 181, 5071-5081 (2008).

63. A. K. Nath et al., Chemical and metabolomic screens identify novel biomarkers and antidotes for cyanide exposure. Faseb J 27, 1928-1938 (2013).

64. H. A. Prag et al., Mechanism of succinate efflux upon reperfusion of the ischaemic heart. Cardiovasc Res 117, 1188-1201 (2021).

Acknowledgements: We thank J. Walker for sharing his knowledge and insights, advice, critical appraisal of the work through the years and critical review of the paper; P. Edelstein for help and advice on statistical analysis and critical review of the paper; D. Tobin and E. Kunji for critical review of the paper; N. Burger for discussion on mass spectrometry assays and results; J. Baeck for toxicity testing of several of the compounds used and preliminary assessments of the effects of some; K. Takaki, J. Fan, and B. Lyu for help with experiments to quantify succinate; N. Goodwin, R. Foster, and the University of Cambridge aquatics facility staff for zebrafish husbandry; and the LMB's media service for preparation of bacterial and tissue culture reagents.

Funding: This work was funded by Wellcome Trust Principal Research Fellowship (223103/Z/21/Z) and the NIH MERIT award (R37 AI054503) to L.R. and the Medical Research Council UK (MC_U105663142) and a Wellcome Trust Investigator award (110159/A/15/Z) to M.P.M. F.J.R. has been supported by the MCIN and "ESF Investing in your Future" RYC2019-027799-I/AEI/10.13039/501100011033 Fellowship since September 2021. **Author contributions:** F.J.R and L.R. designed the project. F.J.R., L.J.W., and H.A.P. performed experiments. F.J.R., L.J.W., H.A.P., L.R., and M.P.M. designed experiments, and analyzed and interpreted data. F.J.R. and L.R. wrote the paper. All authors edited the paper with input from the other authors. **Competing interests:** The authors declare that they have no competing interests.

 Data and Materials availability: All data are available in the main text or the supplementary materials.

List of Supplementary Materials:

Figs. S1 to S5
Tables S1 to S2
Data S1

FIGURE LEGENDS

Figure 1: ETC-derived mROS drive necrosis of Mm-infected macrophages in TNF-high conditions.

(A) Representative pseudocolored confocal images of wild-type (WT) or TNF^{hi} larvae with YFP-expressing macrophages (green), 1 day post infection (dpi) with EBFP2-expresssing Mm (blue), showing MitoTracker Red CM-H_2Xros (magenta) fluorescence. White arrowheads, uninfected macrophages; yellow arrowheads, infected macrophages; yellow arrows, infected macrophages positive for mROS. Scale bar: 20 μm. (B) Quantification of mROS in wild-type or TNF^{hi} larvae 9 hours post-injection of live or heat-killed Mm. Each point represents the mean maximum intensity fluorescence of MitoTracker Red CM-H_2Xros per fish. Black symbols represent macrophages that do not contain bacteria. Red and purple symbols represent Mm-infected and heat-killed Mm-containing macrophages, respectively, in the same animal. Horizontal bars, means; *P<0.05 (one-way ANOVA with uncorrected Dunn's post-test for differences between macrophages in the same animal and with Tukey's post-test for differences between treatments). Representative of two independent experiments. (C to F) Quantification of mROS in larvae 1 dpi with Mm that are wild-type, TNF^{hi} treated with (C) FCCP, (D) DNP, (E) nigericin, or (F) diazoxide, or vehicle. Horizontal bars represent means; ****P<0.0001 (one-way ANOVA with Tukey's post-test). Representative of two-to-three independent experiments.

Figure 2: TNF induces RET mROS at complex I in mycobacterium-infected macrophages.

(A and B) Illustrations of mROS production at complex I during (A) forward electron transport and (B) reverse electron transport. ΔΨ, membrane potential; IMM, inner mitochondrial membrane; I-V, complexes I-V; zigzag arrows, induction; red blunted arrows, inhibition. (C to H) Quantification of mROS in larvae 1 dpi with Mm (C to E) or Mtb (F to H) that are (C) wild-type treated with vehicle or rotenone, (D) wild-type (WT), TNF^{hi} treated with rotenone or vehicle, (E) wild-type, TNF^{hi}, or TNF^{hi} expressing AOX, (F) wild-type or TNF^{hi}, (G) wild-type treated with rotenone or vehicle, (H) wild-type, or TNF^{hi} treated with rotenone or vehicle. Horizontal bars represent means; **P*<0.05, ***P*<0.01, *****P*<0.0001 (one-way ANOVA with Dunn's post-test (C, G, and H), Tukey's post-test (D and E) or uncorrected Dunn's post-test (F)). Black and red symbols in (C, F, and G) represent uninfected (ui) and infected macrophages, respectively, in the same animals. (C to G) representative of two-to-three independent experiments; (H) data from a single experiment.

Figure 3: TNF increases succinate in mycobacterium-infected macrophages.

Quantification of mROS in larvae 1 dpi with Mm that are (A) wild-type (WT), or TNF^{hi} treated with atpenin A, TTFA, DM-malonate, or vehicle (B) wild-type treated with succinate, DEBM, or vehicle. Horizontal bars represent means; **P*<0.05; ***P*<0.01, *****P*<0.0001 (one-way ANOVA with Tukey's post-test (A) or Dunn's post-test (B)). Black and red symbols in (B) represent uninfected (ui) and Mm-infected (Mm) macrophages, respectively, in the same animal. (A and B) representative of two-to-three independent experiments.

Figure 4: TNF-induced glutamine cellular uptake and increased glutaminolysis is responsible for RET and mROS production in mycobacterium-infected macrophages.

(A) Illustration of main metabolic pathways fueling the Krebs cycle with inhibitors used (truncated red arrows). (B to K) Quantification of mROS in larvae 1 dpi with Mm that are (B)

wild-type (WT) or TNF^{hi} treated with GPNA, BPTES, R-162, or vehicle, (C) wild-type treated with GPNA, BPTES, R-162, or vehicle, (D) wild-type or TNF^{hi} treated with telaglenastat or vehicle, (E) wild-type treated with telaglenastat, R-162, or vehicle, (F) wild-type or TNF^{hi} treated with vehicle, or GPNA or R-162 alone or in combination with DM-glutamate, (G) wild-type or TNF^{hi} treated with UK5099 or vehicle, (H) wild-type, or TNF^{hi} treated with perhexiline, 4-BrCA, or vehicle, (I) wild-type treated with UK5099, perhexiline, 4-BrCA, or vehicle, (J and K) wild-type or TNF^{hi} treated with vehicle, or UK5099 or perhexiline (J), or GPNA or R-162 (K) alone or in combination with M-pyruvate. Horizontal bars represent means; *P<0.05; **P<0.01, ***P<0.001, ****P<0.0001 (one-way ANOVA with Tukey's post-test (B, D, F to H, J and K), Dunn's post-test (C, E, and I)). Black and red symbols in (C, E, and I) represent uninfected (ui) and Mm-infected (Mm) macrophages, respectively, in the same animals. (B to D and G to I), representative of two-to-three independent experiments; (E, F, J, and K); data from a single experiment.

Figure 5: TNF-induced glutaminolysis increases succinate levels in mycobacterium-infected macrophages in a RIP3- and PGAM5-dependent manner.

(A and B) Quantification of succinate in zebrafish larvae 1 dpi with Mm or mock-injected, that are (A) wild-type (WT) or TNF^{hi} treated with GPNA, BPTES, or vehicle and (B) TNF^{hi}, TNF^{hi} RIP3 morphants, or TNF^{hi} PGAM5 morphants. Each point represents the mean of four independent experiments in A and two independent experiments in B. Horizontal bars represent pooled SD. ***P<0.001, ****P<0.0001 (one-way ANOVA with Tukey's post-test).

Figure 6: TNF-mediated increased glutamine cellular uptake in mycobacterium-infected increases succinate oxidation, mROS and necrosis.

(A) Representative pseudocolored confocal images of 5 dpi granulomas in wild-type (WT) or TNF^{hi} larvae with YFP-expressing macrophages (green) infected with tdTomato-expressing Mm (magenta). Arrowheads, extracellular cording bacteria. Scale bar: 50 μm. (B) Bacterial cording in wild-type larvae 5 dpi with Mm, treated with vehicle, or succinate or DEBM alone or in combination with diazoxide; $^{**}P<0.01$, $^{***}P<0.001$ (Fisher's exact test). (C) Bacterial cording 5 dpi with Mm in wild-type and TNF^{hi} larvae and wild-type and TNF^{hi} larvae expressing AOX; $^{**}P<0.01$, $^{****}P<0.0001$ (Fisher's exact test). (D) Bacterial cording 5 dpi wild-type or AOX-expressing larvae infected with Mm and treated with succinate, DEBM, or vehicle; $^{*}P<0.05$; $^{**}P<0.01$, $^{***}P<0.001$, $^{****}P<0.0001$ (Fisher's exact test). (E) Number of trunk macrophages in Mm-infected (Mm) larvae and mock-injected (ui) larvae 1 dpi. Horizontal bars represent means; $^{****}P<0.0001$ (one-way ANOVA with Dunn's post-test). (F and G) Percentage of dead THP-1 macrophages at 5 hours post-TNF, treated with (F) rotenone or vehicle starting 1 hour before TNF addition or (G) MitoParaquat (MitoPQ) or vehicle for 5 hours. Black and red symbols represent uninfected (ui) and Mtb-infected macrophages (Mtb), respectively, within the same treatment well. Horizontal bars represent means; $^{*}P<0.05$, $^{**}P<0.01$, $^{****}P<0.0001$ (one-way ANOVA with Tukey's post-test). (H) Schematic diagram showing the role of TNF, mROS and mycobacterial factor(s) in TNF-mediated necrosis of mycobacterium-infected macrophages. (C, D to E, and G) representative of two independent experiments; (B and F) data from a single experiment.

Figure 7: Currently available drugs can intercept TNF-induced mROS production and inhibit necrosis of mycobacterium-infected macrophages.

(A) Representative pseudocolored confocal images of 5 dpi granulomas in larvae with yellow fluorescent macrophages (green) that are wild-type (WT), or TNF^{hi} treated with diazoxide or

vehicle, infected with red fluorescent Mm (magenta). Arrowheads, extracellular cording bacteria. Scale bar: 50 μm. (B to E) Bacterial cording in wild-type or TNF^{hi} larvae 5 dpi with Mm, treated with vehicle or (B) diazoxide, (C) DM-malonate, (D) telaglenastat, or (E) perhexiline. *P<0.05; **P<0.01, ****P<0.0001 (Fisher's exact test). (F) Quantification of mROS in wild-type or TNF^{hi} larvae 1dpi with Mm, treated with metformin, phenformin, or vehicle. Horizontal bars represent means; **P<0.01; ***P<0.001 (one-way ANOVA with Tukey's post-test). (G) Bacterial cording in wild-type or TNF^{hi} larvae 5 dpi with Mm, treated with metformin or vehicle. ****P<0.0001 (Fisher's exact test). (H) Bacterial cording in wild-type larvae 5 dpi with Mm, treated with vehicle, or succinate or DEBM alone or in combination with metformin. *P<0.05; **P<0.01, ***P<0.001 (Fisher's exact test). (I) Quantification of mROS in wild-type or TNF^{hi} 1 dpi with Mtb, treated with metformin or vehicle. Horizontal bars represent means; *P<0.05 (one-way ANOVA with Tukey's post-test). (J) Percentage of dead THP-1 macrophages at 5 hours post-TNF, treated with metformin or vehicle starting 1 hour before TNF addition. Black and red symbols represent uninfected (ui) and Mtb-infected macrophages (Mtb), respectively, within the same treatment well. Horizontal bars represent means; **P<0.01, ****P<0.0001 (one-way ANOVA with Tukey's post-test). (B to G, and I) representative of two independent experiments; (H and J) data from a single experiment.

Figure 1

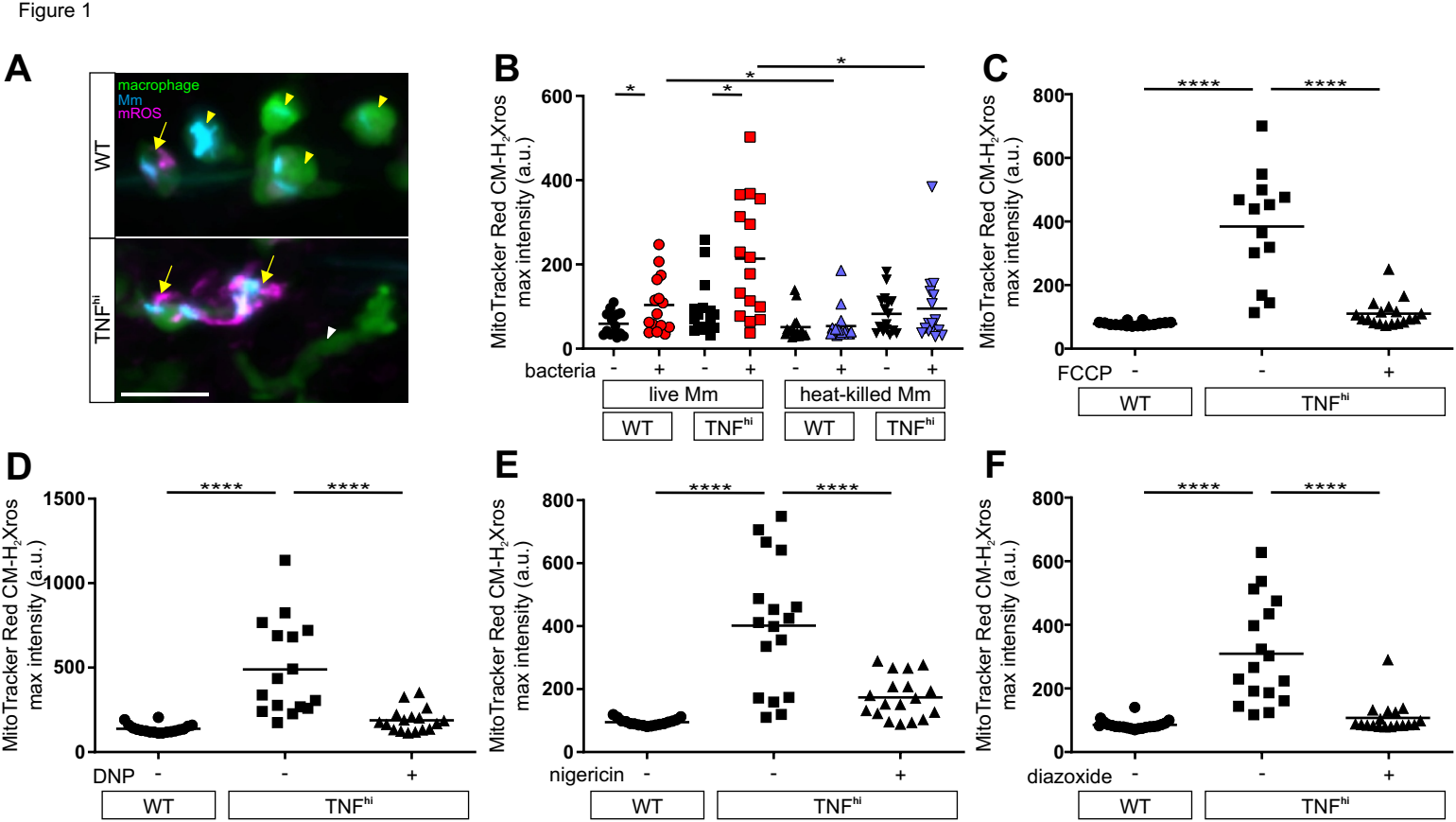
A
macrophage
Mm
mROS
WT
TNFhi
B
MitoTracker Red CM-H2Xros max intensity (a.u.)
bacteria
live Mm
heat-killed Mm
WT
TNFhi
C
FCCP
D
DNP
E
nigericin
F
diazoxide
****

Figure 2

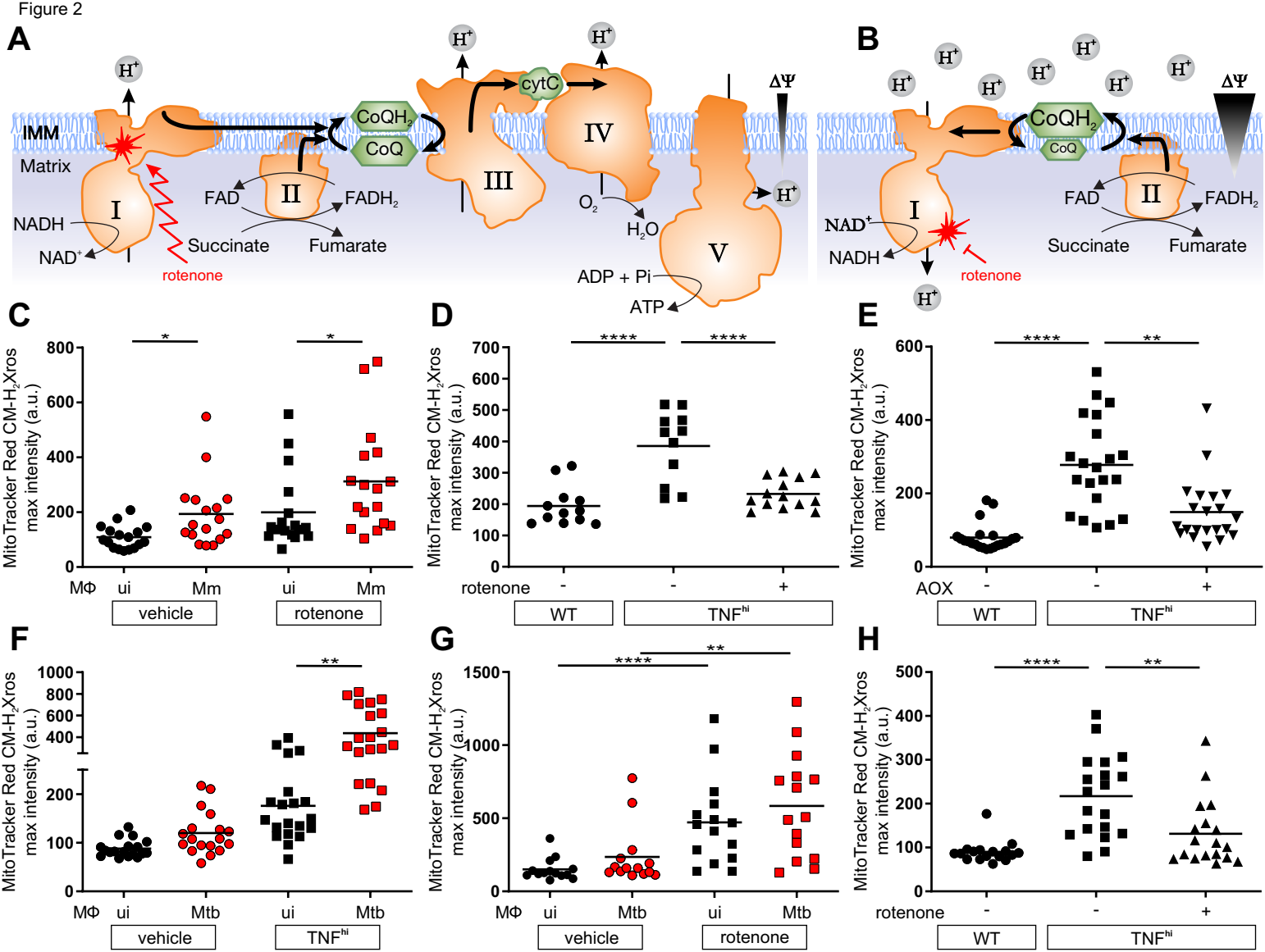
A
B
C
D
E
F
G
H
IMM
Matrix
NADH
NAD+
FAD
FADH2
Succinate
Fumarate
CoQH2
CoQ
cytC
O2
H2O
ADP + Pi
ATP
ΔΨ
rotenone
MitoTracker Red CM-H2Xros max intensity (a.u.)
MΦ
ui
Mm
Mtb
vehicle
rotenone
TNFhi
WT
AOX

Figure 3

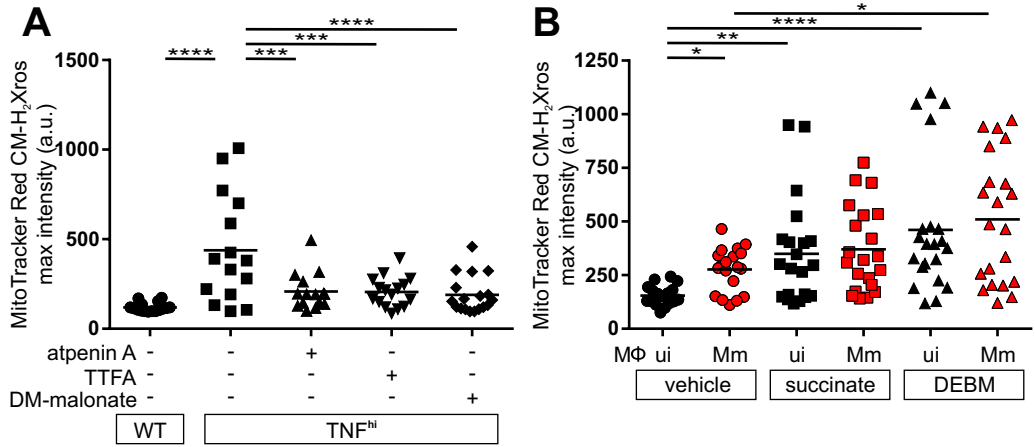
A
MitoTracker Red CM-H2Xros
max intensity (a.u.)
1500
1000
500
0
****
***
****
atpenin A
TTFA
DM-malonate
WT
TNFhi
B
MitoTracker Red CM-H2Xros
max intensity (a.u.)
1250
1000
750
500
250
0
*
**
****
*
MΦ ui Mm ui Mm ui Mm
vehicle
succinate
DEBM

Figure 4

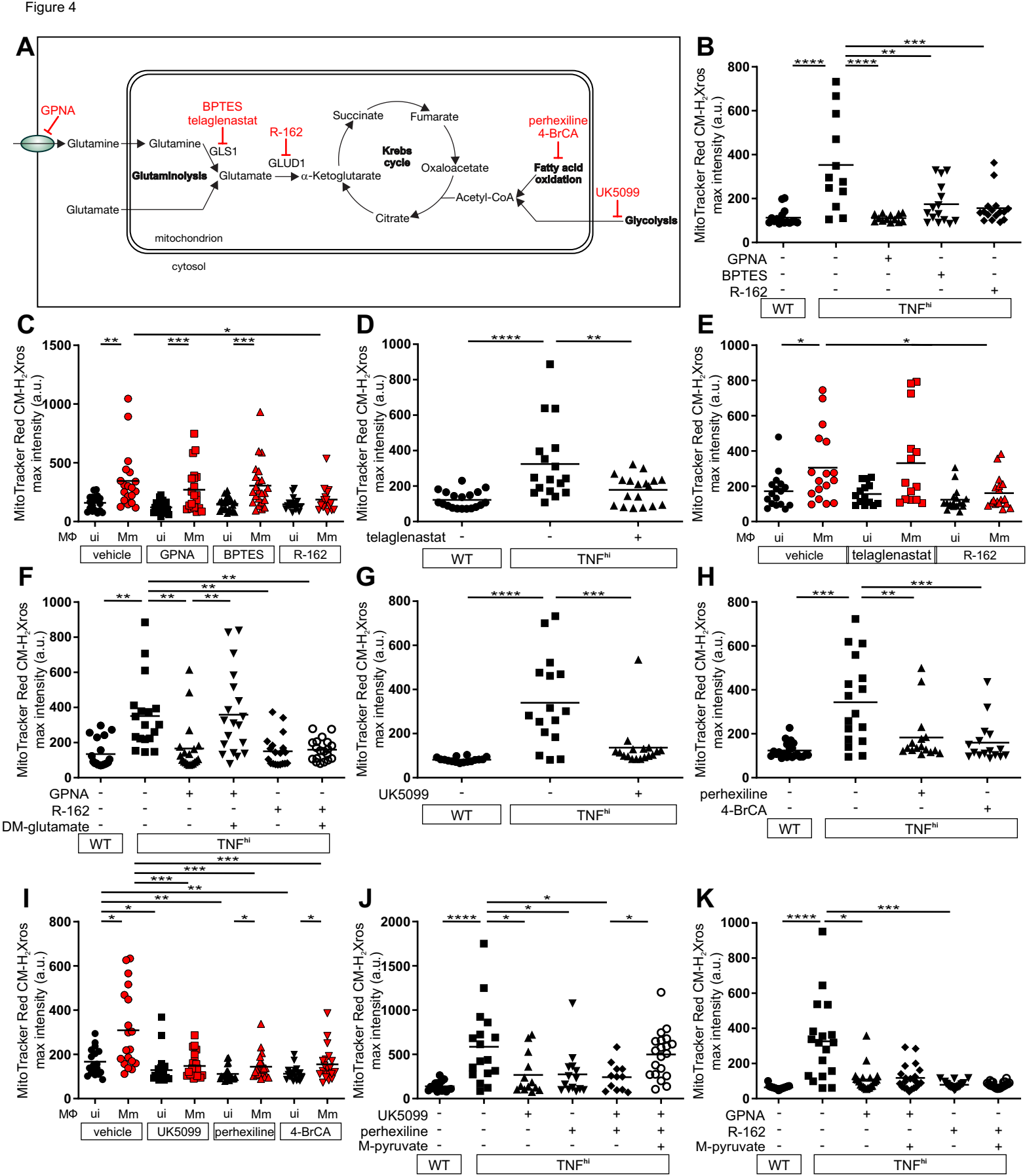
A
GPNA
Glutamine
Glutamine
GLS1
BPTES
telaglenastat
R-162
GLUD1
Glutaminolysis
Glutamate
α-Ketoglutarate
Succinate
Fumarate
Krebs cycle
Oxaloacetate
Acetyl-CoA
Citrate
perhexiline
4-BrCA
Fatty acid oxidation
UK5099
Glycolysis
Glutamate
mitochondrion
cytosol
B
MitoTracker Red CM-H2Xros max intensity (a.u.)
GPNA
BPTES
R-162
WT
TNFhi
C
MΦ
ui
Mm
vehicle
GPNA
BPTES
R-162
D
telaglenastat
WT
TNFhi
E
vehicle
telaglenastat
R-162
F
GPNA
R-162
DM-glutamate
WT
TNFhi
G
UK5099
WT
TNFhi
H
perhexiline
4-BrCA
WT
TNFhi
I
vehicle
UK5099
perhexiline
4-BrCA
J
UK5099
perhexiline
M-pyruvate
WT
TNFhi
K
GPNA
R-162
M-pyruvate
WT
TNFhi

Figure 5

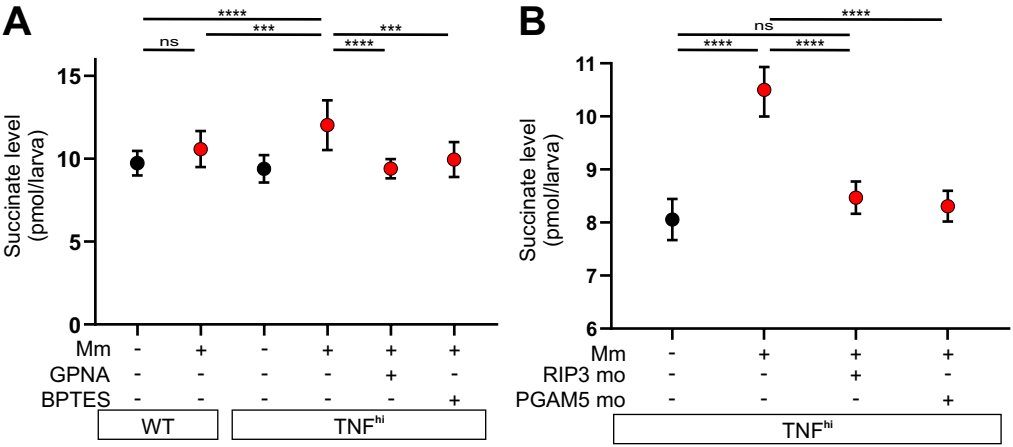
A
Succinate level (pmol/larva)
15
10
5
0
ns
***
****
***
****
Mm - + - + + +
GPNA - - - - + -
BPTES - - - - - +
WT
TNFhi
B
Succinate level (pmol/larva)
11
10
9
8
7
6
ns
****
****
****
Mm - + + +
RIP3 mo - - + -
PGAM5 mo - - - +
TNFhi

Figure 6

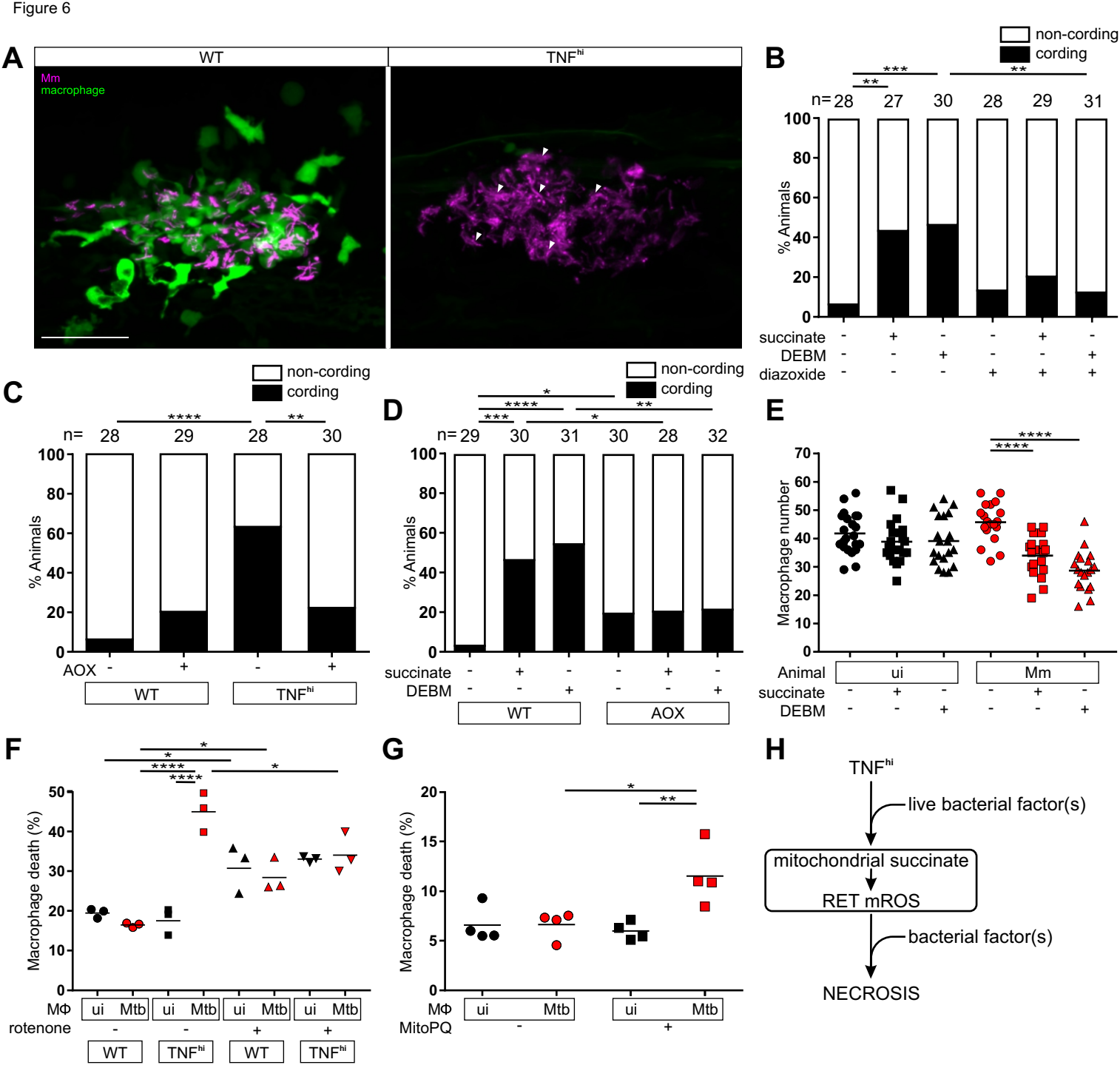
A
WT
TNFhi
Mm
macrophage
B
non-cording
cording
n= 28 27 30 28 29 31
% Animals
succinate
DEBM
diazoxide
C
non-cording
cording
n= 28 29 28 30
% Animals
AOX
WT
TNFhi
D
non-cording
cording
n= 29 30 31 30 28 32
% Animals
succinate
DEBM
WT
AOX
E
Macrophage number
Animal
ui
Mm
succinate
DEBM
F
Macrophage death (%)
MΦ
ui
Mtb
rotenone
WT
TNFhi
G
Macrophage death (%)
MΦ
MitoPQ
H
TNFhi
live bacterial factor(s)
mitochondrial succinate
RET mROS
bacterial factor(s)
NECROSIS

Figure 7

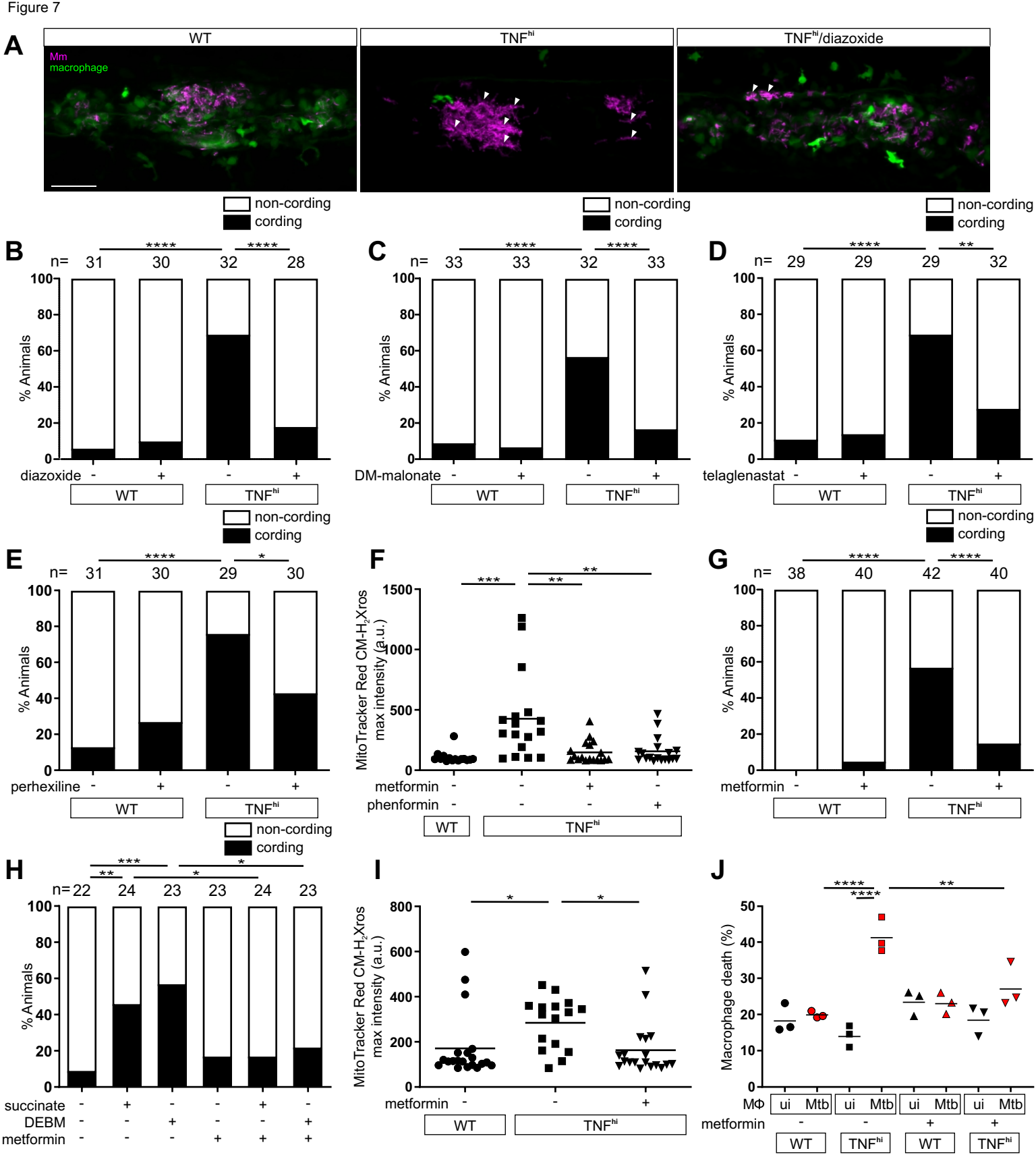
A
WT
TNFhi
TNFhi/diazoxide
Mm
macrophage
non-cording
cording
B
C
D
n=
% Animals
diazoxide
DM-malonate
telaglenastat
WT
TNFhi
E
F
G
perhexiline
MitoTracker Red CM-H2Xros max intensity (a.u.)
metformin
phenformin
H
I
J
succinate
DEBM
Macrophage death (%)
MΦ
ui
Mtb

Science
AAAS

Supplementary Materials for

TNF induces pathogenic mitochondrial ROS in tuberculosis through reverse electron transport

Francisco J. Roca[1,4], Laura J. Whitworth[1,2], Hiran A. Prag[3], Michael P. Murphy[1,3] and Lalita Ramakrishnan[1,2,*]

Correspondence to: lalitar@mrc-lmb.cam.ac.uk

This PDF file includes:

Figs. S1 to S5
Tables S1 to S2
Captions for Data S1

Other Supplementary Materials for this manuscript include the following:

Data S1 (Excel file)

Figure S1

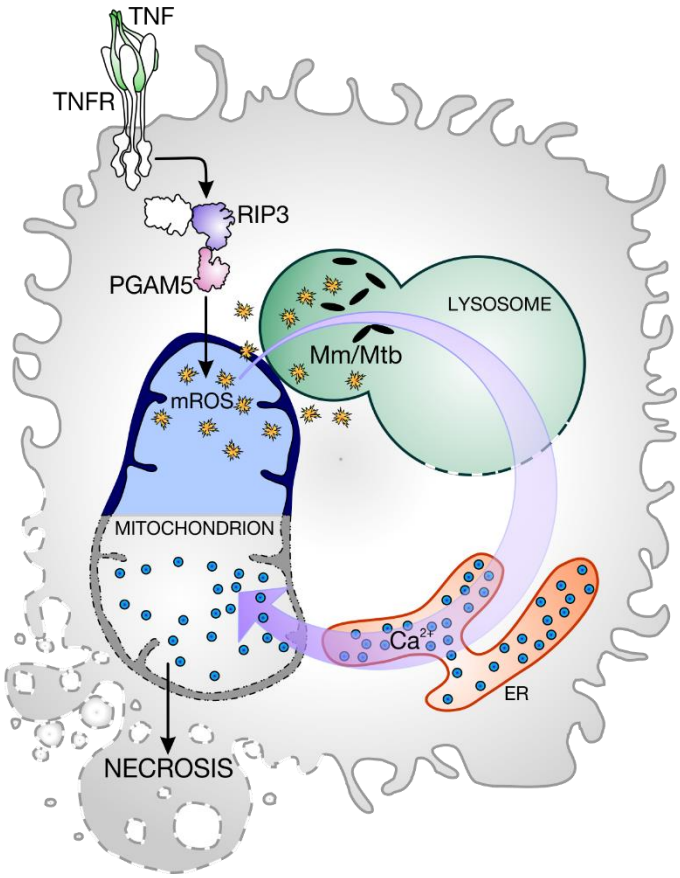

Figure S1.

Excess TNF induces mROS and necrosis of mycobacterium-infected macrophages.

Simplified illustration of the necrosis pathway triggered by excess TNF. Mm, *Mycobacterium marinum*; Mtb, *M. tuberculosis*; ER, endoplasmic reticulum; Ca^{2+}, calcium.

Figure S2

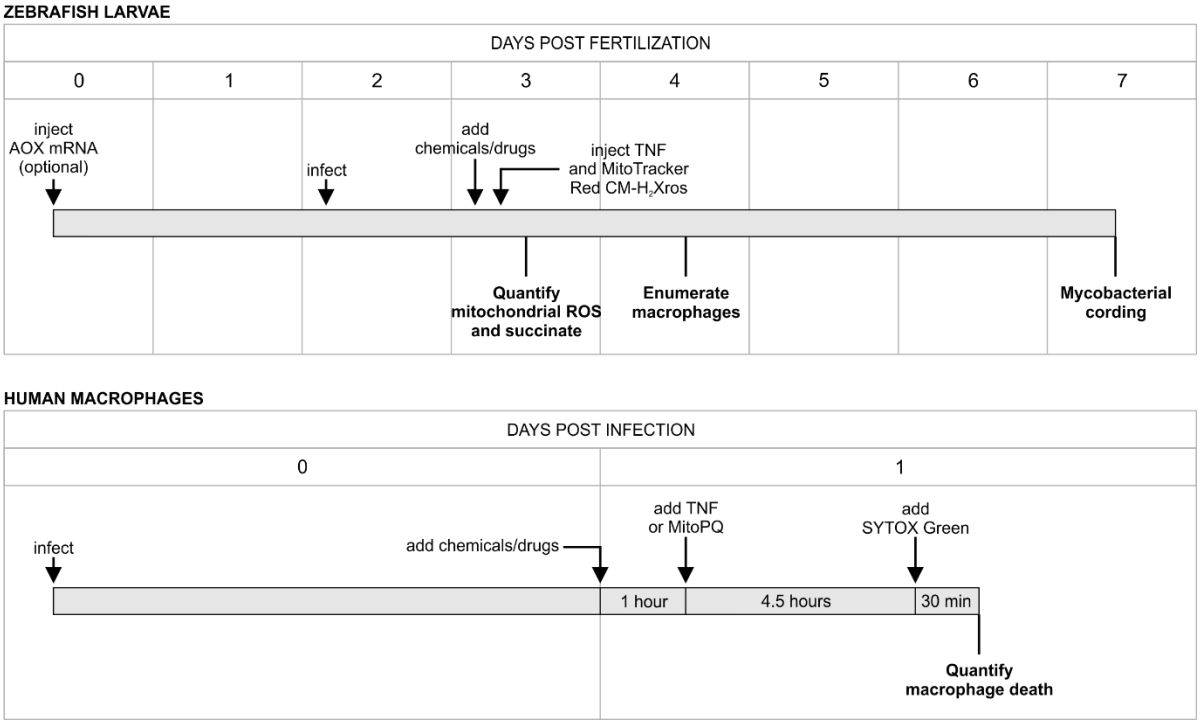

Fig. S2.

Diagram showing the experimental design used in the study in zebrafish larvae and human macrophages.

AOX mRNA, messenger RNA for alternative oxidase from *Ciona intestinalis*; MitoPQ, MitoParaquat. See Materials and Methods for more details about route and time of administration of chemicals, drugs, and TNF in zebrafish larvae.

Figure S3

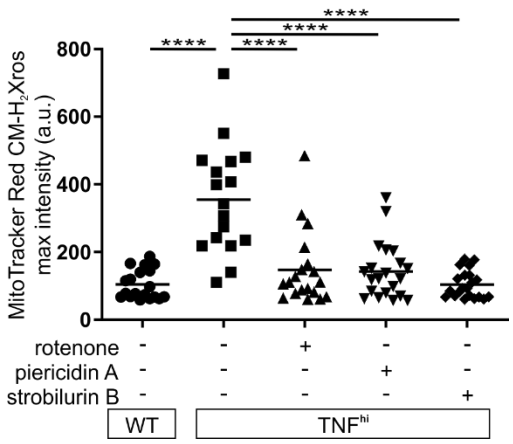

Fig. S3.
Complex I inhibitors with different mechanisms of action reduce mROS in TNF-high conditions.

Quantification of mROS 1 dpi with Mm in larvae that are wild-type (WT) or TNF^{hi} treated with rotenone, piericidin A, strobilurin B, or vehicle. Horizontal bars represent means; ****$P<0.0001$ (one-way ANOVA with Tukey's post-test). Representative of two independent experiments.

Figure S4

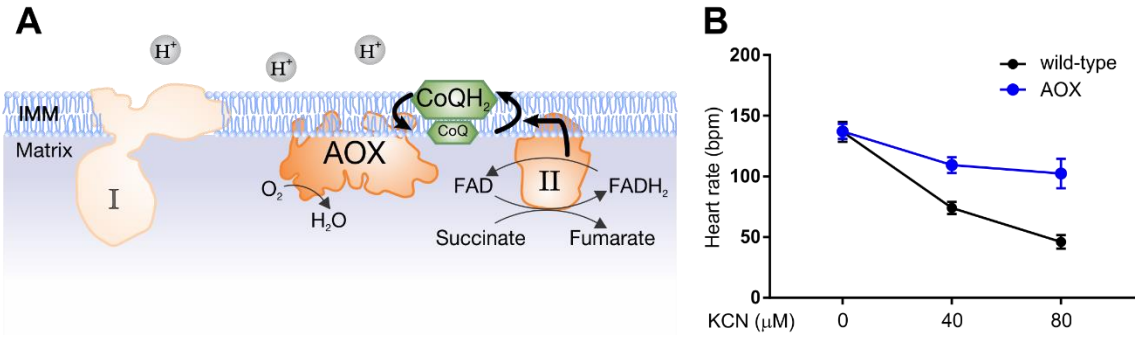

Fig. S4.
AOX-expressing zebrafish larvae are resistant to inhibition of complex IV by cyanide.

(A) Illustration demonstrating how AOX expression decreases the CoQH2 pool and prevents RET mROS production at complex I. Compare with Fig. 2B. AOX, alternative oxidase; IMM, inner mitochondrial membrane; I-II, complexes. (B) Comparison of heart rate (beats per minute) in 3 dpf wild-type or AOX-expressing animals treated with KCN or vehicle. $P<0.0001$ (two-way ANOVA).

Figure S5

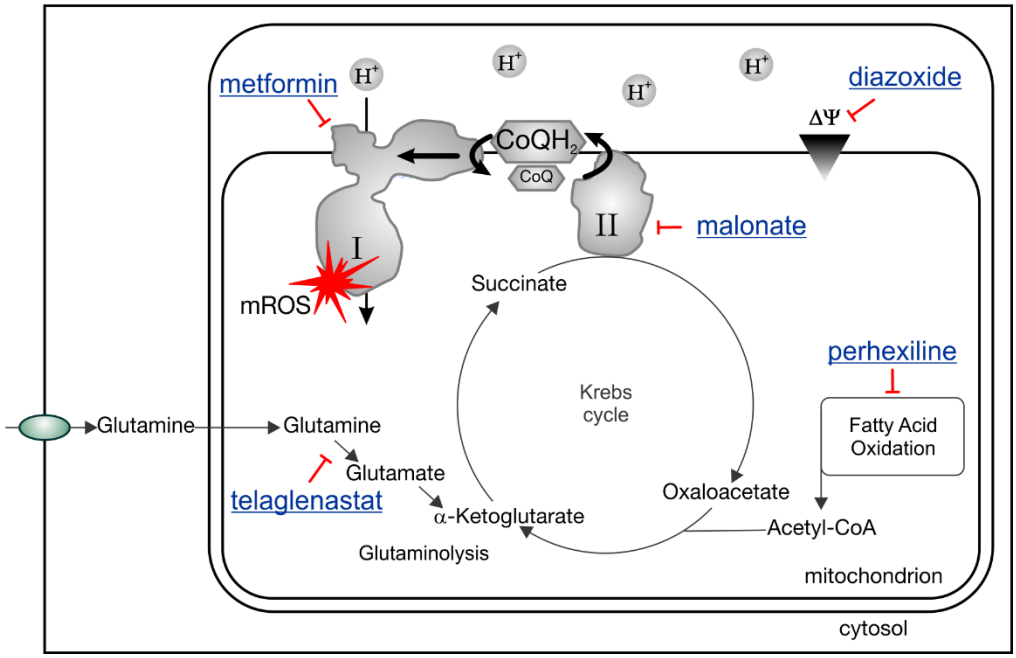

Figure S5.

Currently available drugs can intercept TNF-induced mROS production and inhibit necrosis of mycobacterium-infected macrophages.

Schematic diagram showing the new druggable targets identified in this work to inhibit TNF-elicited RET mROS and necrosis of mycobacterium-infected macrophages. Blue underlined, drugs; red blunted arrows, inhibition.

Compound	Mechanism of action	Human Drug?
Modulators of CI		
Rotenone	Inhibitor of complex I (*12, 14*)	No. Plaguicide in agriculture (*39*)
Piericidin A	Inhibitor of complex I (*14*)	No. Laboratory reagent
Strobilurin B	Inhibitor of complex I (*14*)	No. Fungicide in agriculture (*40*)
Metformin	Inhibitor of complex I (*15*)	Yes, oral, anti-diabetic (*41, 42*)
Phenformin	Inhibitor of complex I (*15*)	No. Withdrawn from clinical use (*41*)
Modulators of CII		
TTFA (thenoyltrifluoroacetone)	Inhibitor of complex II (*43*)	No. Laboratory reagent
Atpenin A5	Inhibitor of complex II (*44*)	No. Laboratory reagent
DM-malonate (dimethyl malonate) as a source of the inhibitor malonate	Inhibitor of complex II (*19*)	Pro-drug shown to prevent ischemia-reperfusion injury in models of heart attack (*28*)
Mitochondrial uncouplers		
FCCP (Carbonyl cyanide-4-(trifluoromethoxy)phenylhydrazone)	Protonophore (*15*)	No. Laboratory reagent
DNP (2.4-dinitrophenol)	Protonophore (*45*)	No. Laboratory reagent
Nigericin	Ionophore, K^+/H^+ exchanger (*15*)	No. Laboratory reagent
Diazoxide	Activator of ATP-sensitive potassium channels (KATP channels) (*46*)	Yes, oral, for hyperinsulinemic hypoglycemia (*47*)
Modulators of glycolysis		
UK5099	Inhibitor of the mitochondrial pyruvate carrier (*48*)	No. Laboratory reagent
Modulators of FAO		
Perhexiline	Inhibitor of CPT1/2 (*49*)	Yes, oral, antianginal (*50*)
4-BrCA (4-Bromocrotonic acid)	Inhibitor of 3-ketoacyl-CoA thiolase (KAT) (*51*)	No. Laboratory reagent
Modulators of glutaminolysis		
GPNA (L-γ-Glutamyl-p-nitroanilide)	Inhibitor of SLC1A5 (Gln transporter) (*52*)	No. Laboratory reagent
BPTES	Inhibitor of glutaminase 1 (GLS1) (*52*)	No. Laboratory reagent
Telaglenastat (CB-839)	Inhibitor of glutaminase 1 (GLS1) (*52*)	Yes, oral, In clinical trials for cancer (*53*)
R-162	Inhibitor of GDH1 (*54*)	No. Laboratory reagent
TCA intermediates and modulators of TCA		
Methyl pyruvate (M-pyruvate)	Cell permeable source of pyruvate (*55*)	No. Laboratory reagent
Diethyl succinate	Cell permeable source of succinate (*19*)	No. Laboratory reagent
DEBM (diethyl butyl malonate)	Inhibitor of the mitochondrial succinate/malate antiporter (*19*)	No. Laboratory reagent

Dimethyl glutamate (DM-glutamate)	Cell permeable source of glutamate (*56*)	No. Laboratory reagent
Others		
MitoParaquat (MitoPQ)	Mitochondria-targeted redox cycler that produces superoxide by redox cycling at the flavin site of complex I (*57*)	No. Paraquat used as herbicide in agriculture (*58*)

Table S1.
Small molecules used in the study.

Compound	Concentration used (tested)	Toxic effects observed
Rotenone	6.25 (6.25-100) nM	Death 24 hours post administration with concentrations > 12.5 nM
Piericidin A	50 (5-500) nM	Necrotic tissues 24 hours post administration with concentrations > 50 nM
Strobilurin B	100 (5-500) nM	Slow heart rate 24 hours post administration with concentrations > 100 nM
Metformin	20 (1-40) μM	Death 24 hours post administration with 40 μM. No toxic effects observed with 20 μM over 4 days
Phenformin	20 (1-40) μM	Gray yolk 24 hours post administration with 40 μM. No toxic effects observed with 20 μM over 4 days
TTFA	1 (0.25-20) μM	Death 24 hours post administration with 5 μM. Curved spines in some larvae 24 hours post administration with 1 μM
Atpenin A5	2.5 (2.5-1000) nM	Necrotic tissues 24 hours post administration with concentrations >2.5 nM and up to 25 nM. Death 4 hours post administration with concentrations >25 nM
dimethyl malonate	10 (1-100) μM	No toxic effects observed for any of the concentrations tested 24 hours post administration. No toxic effects observed with 10 μM over 4 days (not tested for other concentrations)
FCCP	50 (50-500) nM	Necrotic tissues observed in 2 hours with 200 nM. Necrotic tissues 24 hours post administration with 50 nM
2.4-dinitrophenol	100 (10-1000) nM	Necrotic tissues 24 hours post administration with concentrations >500 nM
Nigericin	5 (0.05-5) μM	Death 24 hours post administration with 5 μM
Diazoxide	50 (12.5-2500) nM	No toxic effects observed for any of the concentrations tested 24 hours post administration. No toxic effects observed with 50 nM over a period of 4 days (not tested for other concentrations)
UK5099	10 (1-50) μM	Gray yolk and edema 24 hours post administration with concentrations >10 μM
Perhexiline	10 (0.01-10) μM	No toxic effects observed for the concentrations tested over 4 days
4-Bromocrotonic acid	10 (1-20) μM	No toxic effects observed for the concentrations tested 24 hours post administration
GPNA	10 (0.1-100) μM	No toxic effects observed for the concentrations tested 24 hours post administration
BPTES	5 (2-5) μM	No toxic effects observed for the concentrations tested over 4 days
Telaglenastat	5 (0.5-5) μM	No toxic effects observed for the concentrations tested over 4 days
R-162	1 (0.1-1) μM	No toxic effects observed for the concentrations tested over 4 days

Table S2.

Toxic effects observed in zebrafish larvae after pharmacological interventions.

Data S1. (separate Excel file)
Raw data and summary of the analysis for the experiments showed in Fig. 5, A and B.

Data S1

	uninfected-WT	Mm-WT	uninfected-TNF	Mm-TNF^{hi}	Mm-TNF^{hi}-GPNA	Mm-TNF^{hi}-BPTES
EXPERIMENT 1	10.19964	12.5342	11.56649	15.87831	8.191469	9.621429
	10.25871	10.9107	8.89771	12.96664	9.186496	9.006775
	12.23304	13.3213	9.377055	11.00655	9.754825	9.513851
	10.55048	11.1403	10.29649	12.59976	9.928756	7.913414
	10.75182	10.9969	8.885279	11.56042	10.32894	8.876832
EXPERIMENT 2	8.266625	9.94793	8.52337	11.64261	8.416775	11.22308
	8.31334	9.34203	9.81538	10.46372	7.693635	9.48613
	8.65511	9.42176	9.01085	10.15769	8.581375	11.09407
	7.471995	9.06886	8.863855	9.744265		12.00439
	10.55495	8.39195	9.79467	12.70169		
	8.844005	9.2075	8.69321	13.26537		
EXPERIMENT 3	9.669373	11.9157	10.60354	11.69141	10.28906	9.950385
	9.28354	9.16828	9.64768	10.132	9.7715	11.43472
	9.953755	13.3317	9.425665	11.85374	10.10445	8.064325
	9.63323	10.9463	8.93133	12.69284	10.53676	11.23378
	9.52803	9.16405	9.34577	13.90738		
	10.30629	9.90041	7.994845	12.18015		

	EXPERIMENT 1	EXPERIM	EXPERIMENT 3	COMBINED (with pooled SD)
uninfected-WT				
N	5	6	6	17
mean	10.8	8.68	9.73	9.674117647
SD	0.832	1.03	0.356	0.732714286
Mm-WT				
N	5	6	6	17
mean	11.78	9.23	10.74	10.51294118
SD	1.087	0.5086	1.661	1.085428571
uninfected-TNF				
N	5	6	6	17
mean	9.805	9.117	9.325	9.392764706
SD	1.14	0.5576	0.8572	0.831
Mm-TNF^{hi}				
N	5	6	6	17
mean	12.8	11.33	12.08	12.02705882
SD	1.891	1.44	1.243	1.4985
Mm-TNF^{hi}-GPNA				
N	5	3	4	12
mean	9.478	8.231	10.18	9.40025
SD	0.8283	0.4722	0.3223	0.5805
Mm-TNF^{hi}-BPTES				
N	5	4	4	13
mean	8.986	10.95	10.17	9.954615385
SD	0.6792	1.057	1.551	1.05408

	uninfected-WT-TNF^{hi}	Mm-WT-TNF^{hi}	Mm-RIP3 mo-TNF^{hi}	Mm-PGAM5 mo-TNF^{hi}
EXPERIMENT 1	8.32489811	9.4561594	7.75383391	8.53134
	9.220129	10.1714924	7.62524815	7.60957
	8.0947494	9.222644	8.492279	7.42046
	8.0255603	10.757272	8.42630054	8.83444
	7.4381754	9.78669832	8.33939946	8.18587
	7.42469075	11.0531316	8.84089999	8.49575
EXPERIMENT 2	7.42881553	11.6159017	9.1216251	8.45264
	8.48136285	9.9865356	8.5747611	8.54323
	8.15280383	10.7075206	9.0975498	8.12821
	8.39264242	10.9007516	8.9212862	8.49751
	7.62696943	11.5066377	7.7993937	7.9872
			8.6476334	8.99449

	EXPERIMENT 1	EXPERIMENT 2	COMBINED (with pooled SD)
uninfected-WT-TNF^{hi}			
N	6	5	11
mean	8.088	8.017	8.055727273
SD	0.6639	0.4672	0.576477778
Mm-WT-TNF^{hi}			
N	6	5	11
mean	10.07	10.94	10.46545455
SD	0.7244	0.66	0.695777778
Mm-RIP3 mo-TNF^{hi}			
N	6	6	12
mean	8.246	8.694	8.47
SD	0.4655	0.4928	0.47915
Mm-PGAM5 mo-TNF^{hi}			
N	6	6	12
mean	8.18	8.434	8.307
SD	0.5575	0.3532	0.45535